Spatiotemporal variations in summertime Arctic aerosol optical depth caused by synoptic-scale atmospheric circulation in three reanalyses

Akio Yamagami[1], Mizuo Kajino[1], Takashi Maki[2], and Takahiro Toyoda[3]

[1]Meteorological Research Institute
[2]MRI, japan
[3]Meteorological Research Institute, Japan Meteorological Agency

December 7, 2022

Abstract

Atmospheric aerosols influence the radiation budget, cloud amount, cloud properties, and surface albedos of sea ice and snow over the Arctic. In spite of their climatic importance, Arctic aerosol contains large uncertainties due to limited observations. This study evaluates the Arctic aerosol variability in three reanalyses, JRAero, CAMSRA, and MERRA2, in terms of the aerosol optical depth (AOD), and its relationship to the atmospheric disturbances on synoptic timescales. The AOD becomes highest in July–August over most of the Arctic regions, except for the North Atlantic and Greenland, where monthly variability is rather small. The three reanalyses show a general consistency in the horizontal distribution and temporal variability of the total AOD in summer. In contrast, the contributions of individual aerosol species to the total AOD are quite different among the reanalyses. Compared with observations, the AOD variability is represented well in all reanalyses in summer with high correlation coefficients, albeit exhibiting errors as large as the average AOD. The composite analysis shows that large aerosol emissions in Northern Eurasia and Alaska and transport by a typical atmospheric circulation pattern contribute to the high aerosol loading events in each area of the Arctic. Meanwhile, the empirical orthogonal function analysis depicts that the first- and second-largest AOD variabilities on the synoptic timescales appear over Northern Eurasia. Our results indicate that these summertime AOD variabilities mainly result from aerosol transportation and deposition due to the atmospheric disturbances on synoptic scales, suggesting an essential role played by Arctic cyclones.

Spatiotemporal variations in summertime Arctic aerosol optical depth caused by synoptic-scale atmospheric circulation in three reanalyses

A. Yamagami[1], M. Kajino[1,2], T. Maki[1], and T. Toyoda[1]

[1] Meteorological Research Institute (MRI), Japan Meteorological Agency (JMA), Tsukuba, Ibaraki, 305-0052, Japan

[2] Faculty of Life and Environmental Sciences, University of Tsukuba, Tsukuba, Ibaraki, 305-8572, Japan

Corresponding author: Akio Yamagami (yamakami@mri-jma.go.jp)

†Additional author notes should be indicated with symbols (current addresses, for example).

Key Points: (140 characters limit)

- Three aerosol reanalyses (JRAero, CAMSRA, and MERRA2) showed consistent distributions for summertime total AODs over the Arctic.
- The synoptic variability of summertime total AODs in the reanalyses correlated well with satellite observations in the Arctic ($R \geq 0.6$).
- Synoptic disturbances dominate the poleward transport, aging and deposition of aerosols, suggesting the importance of Arctic cyclones.

Abstract (250 words limit)

Atmospheric aerosols influence the radiation budget, cloud amount, cloud properties, and surface albedos of sea ice and snow over the Arctic. In spite of their climatic importance, Arctic aerosol contains large uncertainties due to limited observations. This study evaluates the Arctic aerosol variability in three reanalyses, JRAero, CAMSRA, and MERRA2, in terms of the aerosol optical depth (AOD), and its relationship to the atmospheric disturbances on synoptic timescales. The AOD becomes highest in July–August over most of the Arctic regions, except for the North Atlantic and Greenland, where monthly variability is rather small. The three reanalyses show a general consistency in the horizontal distribution and temporal variability of the total AOD in summer. In contrast, the contributions of individual aerosol species to the total AOD are quite different among the reanalyses. Compared with observations, the AOD variability is represented well in all reanalyses in summer with high correlation coefficients, albeit exhibiting errors as large as the average AOD. The composite analysis shows that large aerosol emissions in Northern Eurasia and Alaska and transport by a typical atmospheric circulation pattern contribute to the high aerosol loading events in each area of the Arctic. Meanwhile, the empirical orthogonal function analysis depicts that the first- and second-largest AOD variabilities on the synoptic timescales appear over Northern Eurasia. Our results indicate that these summertime AOD variabilities mainly result from aerosol transportation and deposition due to the atmospheric disturbances on synoptic scales, suggesting an essential role played by Arctic cyclones.

Plain Language Summary (200 words limit)

Arctic warming is particularly faster than global warming; hence aerosols are considered one of the most important factors for the Arctic climate system. Aerosols can change the radiation budgets through aerosol–radiation and aerosol–cloud interactions, and changing the surface albedo over snow and sea ice over the Arctic. This study evaluates the Arctic aerosol variability in three reanalyses (JRAero, CAMSRA, and MERRA2) in terms of the aerosol optical depth (AOD), and its relationship to the atmospheric disturbances on synoptic timescales. The AOD becomes highest in July–August over most of the Arctic regions. The three reanalyses show a general consistency in the horizontal distribution and temporal variability of the total AOD in summer. In contrast, the contributions of individual aerosol species to the total AOD are quite different among the reanalyses. The largest contributions to the total AOD were organic carbon. The summertime AOD variability is generally represented in all reanalyses, albeit exhibiting an error as large as the average AOD. The maximum AOD variability appears over Northern Eurasia on the synoptic timescales. The generation and development of summertime Arctic cyclones and associated moisture and precipitation play essential roles in aerosol transportation and deposition over the Arctic.

1 Introduction

The atmospheric aerosols have attracted much interest because they have significant influences on climate change and human health (IPCC, 2021). Arctic warming is particularly faster than global warming (Yoshimori et al., 2014; Kaufman and Feldl, 2022). In relation to this, aerosol is considered as one of the most important factors for the Arctic climate system, since aerosols can change the radiation budgets through aerosol–radiation (direct effect) and aerosol–cloud (indirect effect) interactions (Haywood and Boucher, 2000; Lohmann and Feichter, 2005). In addition to these two main influences on the atmosphere, absorbing aerosols can change the surface albedo over snow (Warren and Wiscombe, 1980) and sea ice (Perovich et al., 1998) areas, which would also contribute to accelerate the Arctic atmosphere warming. Comparable to warming by greenhouse gases and natural climate variability, Arctic aerosols affect the past (Aizawa et al., 2021) and future Arctic climate (Im et al., 2021). DeRepentigny et al. (2022) showed that the interannual variability of biomass burning (BB) over the mid to high latitude has enhanced the sea ice decrease and the surface warming over the Arctic in the 21st century through nonlinear aerosol–cloud interactions and ice–albedo feedback.

Numerous studies pointed out that BB aerosols play an important role in the variation of Arctic aerosols, especially black carbon (BC) aerosol, through the transportation and wet removal processes (Garrett et al., 2010, 2011; Stohl, 2006; Stohl et al., 2006, 2013). Mori et al. (2020, 2021) showed that BB largely affected the seasonal variation of BC at the Barrow station, but it had only a small influence at the Ny-Ålesund station. They also showed the correlation coefficient in seasonal variability of the BC mass concentration between ambient air and surface were higher at the Ny-Ålesund than at Barrow because of the difference in wet deposition fluxes due to precipitation. Creamean et al. (2021) also depicted the importance of wet removal processes on the vertical profiles of clouds and aerosols by balloon observations at Oliktok Point in Alaska. Schmale et al. (2022) analyzed the seasonal cycle and the long-term trend of the mass concentration of nine aerosol species and four optical properties at 10 observational sites over the Arctic. Their results suggested that while most of the aerosol species showed a significant decline trend in spring, the significant trend was not uniform among the sites in summer. The scattering coefficient in summer showed a decreasing trend at the Barrow/Utqiagvik and Zeppelin sites. These long-term observations are mainly obtained at surface stations in the south of 70°N.

Short-term observation campaigns from aircrafts and ships provide important information about Arctic aerosols in upper air and further north regions. Bossioli et al. (2021) investigated the influence of polluted air intrusion to the Arctic from BB and anthropogenic sources on the aerosol–radiation and aerosol–cloud interactions by using a Weather and Research and Forecasting (WRF) model fully coupled with a chemical transport model (CTM; Grell et al., 2005) from 25 July to 9 August 2014. Their results showed that the combination of both BB and anthropogenic sources can lead to significant changes in the cloud liquid water, cloud droplet concentration, and radiation budget. Porter et al. (2022) reported highly active ice-nucleating particles (INPs) observed over the North Pole in August to September 2018, which were the biological INPs supplied from the terrestrial source over the Russian coast and the oceanic source from the open water area. While their back trajectory analysis showed little contribution from the marginal ice zone (MIZ), Inoue et al. (2021) suggested that wind-driven oceanic waves could supply biological INPs at the MIZ.

In addition to observational studies, numerous modeling studies were conducted to enhance our understanding of atmospheric chemical processes at the regional (Kajino et al., 2019a, 2021a, b; Grell et al., 2005) and global (Bhattacharjee et al., 2018; Gong et al., 2012; Morcrette et al., 2009; Rémy et al., 2019; Tanaka, 2003; Tanaka and Chiba, 2005) scales. CTMs were also used with data assimilation (Benedetti et al., 2009; Sekiyama et al., 2011; Yumimoto et al., 2016) and inversion method (Maki et al., 2011; Sugimoto et al., 2010; Yumimoto et al., 2008) to estimate the spatiotemporal distribution and emission. These studies bridged observational and modeling studies by providing the atmospheric aerosol reanalysis. The climatology of the aerosol optical properties in reanalyses was also used as the aerosol influence on the atmosphere in operational numerical weather prediction (NWP) models (Bozzo et al., 2020; Japan Meteorological Agency (JMA), 2019). Numerous studies showed that the improvement of aerosol treatment enhances the forecast skill of operational NWP on short- to sub-seasonal timescales (Benedetti and Vitart, 2018; Jeong, 2020; Mulcahy et al., 2014; Rodwell and Jung, 2008). Besides, some forecast errors (e.g., surface to lower-troposphere temperature forecast errors) are related to a simple aerosol treatment in NWP models (Huang and Ding, 2021; Rémy et al., 2015; Yamagami et al., 2022; Zhang et al., 2016).

The reanalyses provide spatial and temporal uniform aerosol data over the globe. That is one of the significant advantages of understanding aerosol behaviors over the Arctic, where sparse observation network, while there are few studies were conducted using aerosol reanalyses. Xian et al. (2022) investigated the monthly variability and long-term trend of aerosol optical depth (AOD) over the Arctic in spring and summer by employing satellite and surface observations and aerosol reanalyses. Their results showed the monthly climatological variabilities and negative (positive) trends in spring (summer) in aerosol reanalyses were similar to those in the satellite observation over the Arctic. Chakraborty et al. (2021) applied the atmospheric river (AR) concept to the AOD (aerosol AR; AAR) through aerosol reanalysis and showed that the climatology of the AAR had a Northern Eurasia to North Pole direction, especially carbonaceous and sulfate aerosols.

The synoptic-scale disturbances over the Arctic were most frequently observed in summer (Crawford and Serreze, 2016; Tilinina et al., 2014; Serreze and Barret, 2008; Vessey et al., 2020; Zhang et al., 2004). The Arctic cyclones (ACs) in summer have a different three-dimensional (3D) structure from mid-latitude cyclones (Tanaka et al., 2012) and wintertime ACs (Clancy et al., 2021). Gray et al. (2021) presented the difference in the structures of the summertime ACs caused by their relationship to the tropopause polar vortex. Although Xian et al. (2022) suggested that the AC frequency might not contribute to the Arctic AOD trend because the AC frequency had no significant trend (Vessey et al., 2020), the AC activity will influence the Arctic aerosol variability on the synoptic timescales; for example, ACs can contribute to the emission, transport, aging, and removal processes (e.g., wet deposition) of Arctic aerosols. Although previous studies provided some suggestions as regards the contribution of the Arctic aerosol variability and the synoptic activities over the Arctic, no study has yet focused on the relationship between Arctic aerosol and ACs in summer.

In this study, we investigated the relationship between the atmospheric circulation and the Arctic aerosol variabilities, especially the relationship between ACs and AOD, by using global aerosol reanalyses. We also assessed the uncertainties by conducting an intercomparison of the global aerosol reanalyses over the Arctic.

2 Data and Methods

This study used the AOD at 550 nm from three aerosol reanalyses: 1) Japanese Reanalysis for Aerosols (JRAero) v1.0 (Yumimoto et al., 2017) provided by Kyushu University and the Meteorological Research Institute (MRI); 2) Copernicus Atmosphere Monitoring Service reanalysis (CAMSRA; Inness et al., 2019); and 3) and Modern-Era Retrospective Analysis for Research and Applications version 2 (MERRA2; Gelaro et al., 2017).

The JRAero system is based on the JMA Earth System Model version 1 (JMA-ESM1; Yukimoto et al., 2011) comprising the atmospheric general circulation model (MRI-AGCM3) and the Model of Aerosol Species In the Global AtmospheRe mk-2 (MASINGAR mk-2; Tanaka et al., 2003). The horizontal wind and the temperature predicted by MRI-AGCM3 were nudged to the six-hourly JMA operational global analysis (GANAL/JMA). MASINGAR mk-2 then calculated the emission, transport, reaction, and deposition of five major aerosol species (i.e., sulfate, BC, organic carbon (OC), mineral dust, and sea salt (SS) aerosols) by using the atmospheric fields. MRI-AGCM3 received the mixing ratio and the deposition flux of these aerosol species and calculated the aerosol–radiative interaction and the change of the surface condition at each timestep (900 s). MASINGAR-mk2 discretized mineral dust and SS aerosols into 10-size bins and assumed lognormal size distributions for other aerosol components. The JRAero system assimilated the MODIS AOD observation provided by the US Naval Research Laboratory and the University of North Dakota from 40°S to 60°N by a two-dimensional variational method. After the AOD assimilation, the 3D extinction coefficient was modified by weighting the predicted mixing ratio; thus, the vertical profile of the predicted aerosol mixing ratio was kept during the assimilation. JRAero provides the AOD with TL159 (~1.1° × 1.1°) horizontal interval and 48 vertical levels. Yuminoto et al. (2017), Yukimoto et al. (2011, 2012), Tanaka et al. (2003), and Tanaka and Chiba (2005) provided more detailed information on JRAero, MRI-ESM1, and MASINGAR mk-2.

CAMSRA is the latest aerosol reanalysis provided by the European Centre for Medium-Range Forecast after the MACC and CAMS interim (Inness et al., 2019). It is based on the Integrated Forecast System (IFS), Cy42r1, which contains the Carbon Bond 2005 chemistry scheme (CB05) and is referred to as IFS(CB05) (Flemming et al., 2015). The chemistry scheme module calculates the aerosol and gas reaction, transport, and deposition. IFS(CB05) has a horizontal resolution of T255 (~0.7° × 0.7°) and 60 hybrid sigma-pressure levels up to 0.1 hPa. As with JRAero, CAMSRA provides the five major aerosol species and chemical gases (i.e., three bins of SS and dust, hydrophobic and hydroscopic organic matter, BC, sulfate aerosol, and gas-phase sulfate dioxide). While the observations for individual chemical gas components (i.e., O_3, CO, and NO_2) are assimilated, the total AOD observed from AATSR (December 2012–March 2012) and MODIS Terra and Aqua (January 2011–December 2016) is assimilated by a four-dimensional variational method regarding aerosol component. The observed data at >70°N are rejected to assure the observational data quality. ERA5 (Hersbach et al., 2020) provides atmospheric fields, while CAMSRA provides radiation fields, including the effect of chemical gases and aerosol influences. Please refer to Inness et al. (2019) for further details on the CAMSRA.

MERRA2 has the longest period in these three reanalyses (1980–onward) provided by the NASA Global Modeling and Assimilation Office. MERRA2 is based on the Goddard Earth

Observing System, Version 5 (GEOS-5) atmospheric model coupled with the Goddard Chemistry, Aerosol, Radiation, and Transport model (GOCART; Chin et al., 2002; Colarco et al., 2010). The GOCART models treat five aerosol species (i.e., five bins dust and SS, hydrophobic and hydrophilic OC and BC, and sulfate aerosols). MERRA2 assimilates the bias-corrected AOD observed by Advanced Very High Resolution Radiometer instruments (Heidinger et al., 2014), Multiangle Imaging Spectro Radiometer, MODIS Terra and Aqua, and ground-based Aerosol Robotic Network. In the assimilation system of MERRA2, the analysis increment for the mixing ratio of each aerosol (3D field) is calculated from the analysis increment of the total AOD (2D field) every 3h. Therefore, the first guess of the 3D mixing ratio is directly updated using the analysis increment of the mixing ratio, in contrast to JRAero, in which the vertical profile of the mass mixing ratio is kept during the assimilation. The original model grid in MERRA2 is roughly 50 km in horizontal and 72 vertical levels from the surface to 0.01 hPa. MERRA2 product is provided with regular 0.5° latitude and 0.625° longitude horizontal grid. Galero et al. (2017) presented an overview of MERRA2, including both atmospheric and aerosol representations. Buchard et al. (2017) and Randles et al. (2017) provided more details on the aerosol evaluations in MERRA2.

We used the six-hourly AOD during the 2011–2017 period, a common period for the three reanalyses. The original six-hourly AOD was utilized for the intercomparison and verification of the reanalyses, whereas the AOD with a band-pass filter by the 3- and 14-day running means (i.e., the 14-day running mean removed and then the 3-day running mean applied) was used for the composite and empirical orthogonal function analysis (EOF) analyses to focus on the synoptic timescale variability.

We also used the MODIS AOD (Remer et al., 2005; Levy et al., 2007) in the same period to verify the AOD in the reanalyses. The atmospheric fields were obtained from JRA-55 (Kobayashi et al., 2015).

3 Results

3.1 Comparison of the Arctic AOD in JRAero, CAMSRA, and MERRA2

We first calculated the area-averaged aerosol variability over each region in the Arctic in JRAero (Fig. 1). The area-averaged AOD over the north of 60°N (N60, Fig. 1a) showed the highest values of ~0.15 in July and August. The AOD peak in July disappeared at the average of the north of 70°N (Arctic, Fig. 1b), indicating that the high aerosol loading reached the high latitude area only in August. As with the N60 and Arctic, Northern Eurasia (NEurasia, Fig. 1d), Chukchi (Fig. 1e), and Canadian Arctic Archipelago (CAA, Fig. 1f) showed AOD peaks in July and August. The results indicated that the aerosol loading in these areas mainly contributed to the monthly variability of the AOD over N60 and Arctic (Figs. 1a and b). The AOD in Greenland (Fig. 1g) depicted a similar variability to these areas, with its magnitude smaller than that in the other regions. In contrast, no peak was observed in July nor August in Northern Atlantic (NAtlantic, Fig. 1c).

Among the five aerosol species, the OC contribution was the largest on the total AOD in N60 and Arctic in summer. OC and BC had more than half of the contribution over NEurasia, Chukchi, CAA, and Greenland in July and August. In NAtlantic, the OC contribution had a peak in August, whereas the decrease of the OC contribution in the other season was compensate for the increase of the SS contribution, resulting in the weak seasonal variability in total AOD. Such seasonal variability in the SS contribution was not observed in other regions, indicating the dominance of oceanic sources over the NAtlantic. Seasonal variability of the sulfate aerosol was also small in all areas, except in NEurasia, where its contribution on the total AOD variability was the largest in winter. Dust aerosol had the smallest contribution, even in spring.

The six-hourly total AOD in CAMSRA and MERRA2 showed the largest values in July and August over N60, consistent with that in JRAero (Fig. 2a). The median and the average in JRAero were slightly larger than those in CAMSRA and MERRA2. In addition, although the 10^{th} percentile values were almost similar among the reanalyses, the range from the 10^{th} to the 90^{th} percentile values was broader in JRAero than in CAMSRA and MERRA2. However, the range from the 25^{th} to the 75^{th} percentile values in JRAero was comparable to that in the two reanalyses. These results indicated that the total AOD in JRAero had a large variability compared to the other reanalyses and some extreme AOD values. As discussed below, some part of the high AOD events were associated with the synoptic disturbances over the Arctic. Despite these differences, the six-hourly variability of the total AOD in spring and summer was basically consistent among the three reanalyses.

In contrast to the total AOD, the individual aerosol contributions were quite different among the reanalyses (Figs. 2b–f). In all reanalyses, the OC had the largest contributions on the total AOD in July and August (Fig. 2d). Although the average and median values of OC in JRAero were comparable to those in MERRA2, CAMSRA showed larger values than these two reanalyses. BC showed a similar relationship among the reanalyses (Fig. 2c). The histograms of sulfate (Fig. 2b) and SS (Fig. 2f) in JRAero showed much larger contributions and variabilities than those in CAMSRA and MERRA2. The first and second largest contributions to the total AOD (Fig. S1) were OC (JRAero, CAMSRA, and MERRA2: ~15–60%, ~55–70%, and ~30–70%) and sulfate (JRAero, CAMSRA, and MERRA2: ~10–60%, ~15–25%, and ~15–40%). The

SS contribution was also remarkable in JRAero (~10–40%), which was comparable to the contribution of sulfate. The results implied that the two aerosols compensated for the smaller contribution of OC in JRAero because the total AOD was bound by the MODIS AOD assimilation (Flemming et al., 2017). Although the variability of sulfate was similar between CAMSRA and MERRA2 in July and August, the former showed a generally larger value than the latter (e.g., the 75th percentile value in CAMSRA was similar to the 25th percentile value in MERRA2). Assuming that the atmospheric fields and emission are almost similar among the reanalyses, the differences in sulfate are possibly related to the removal processes, especially in JRAero. CAMSRA also showed a larger contribution from dust aerosol than JRAero and MERRA2 (Fig. 2e). Almost similar differences were observed from April to June.

From October to March, a difference among the reanalyses was found, even in the total AOD; the total AOD in CAMSRA was much smaller than those in JRAero and MERRA2 (Fig. 2a). In addition to the total AOD, the contribution of the individual species was also different among the reanalyses in these months (e.g., dust aerosol in CAMSRA and sulfate and SS aerosols in JRAero). The available observational data became small due to the polar night over the high latitudes in the Northern Hemisphere; hence, the AOD over the Arctic in late autumn to early spring highly depended on the CTMs in each reanalysis, consequently leading to a difference in the AOD. These results suggest that the reanalyses was less reliable in late autumn to early spring, while they provided a reliable value in terms of the total AOD in spring and

summer over the Arctic. Still, we need careful treatment for using individual aerosol species in the reanalyses. Thus, the analyses in this study mainly focused on the total AOD.

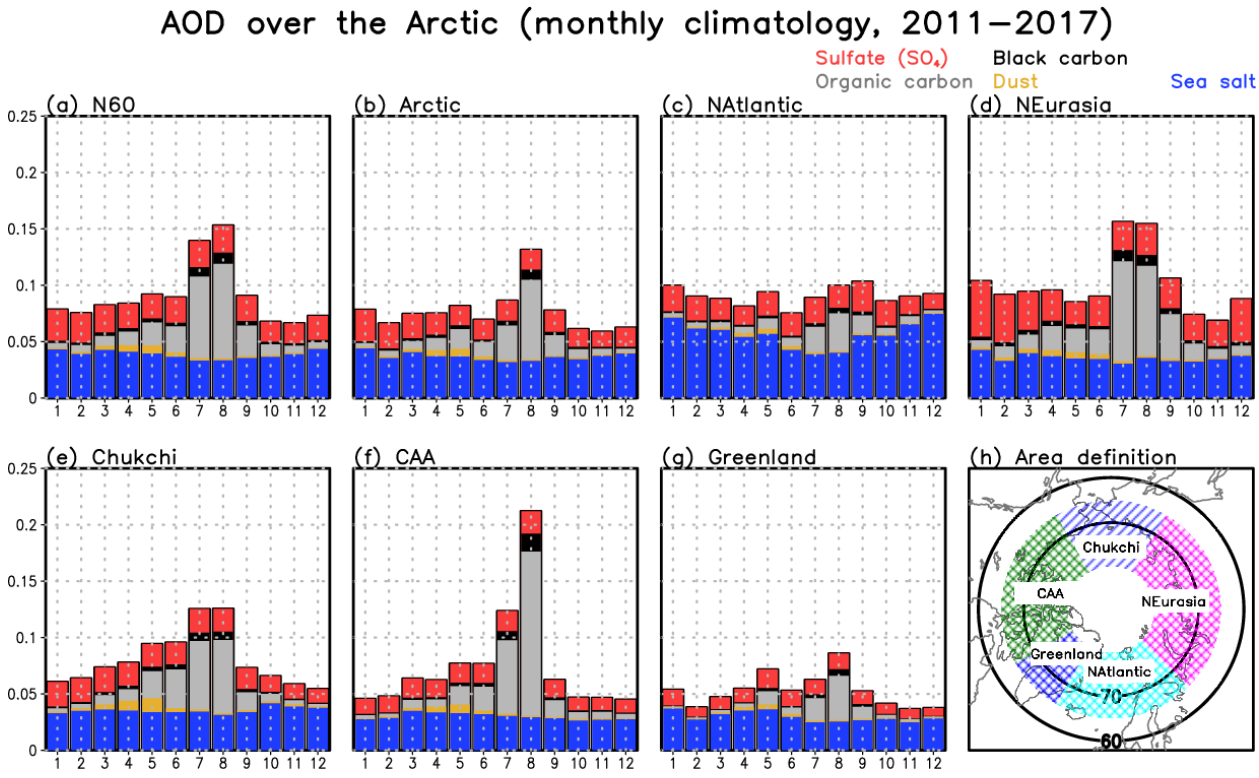

Figure 1 (a–g) Monthly climatological AOD in JRAero averaged over (a) North Pole (≥60°N), (b) Arctic (≥70°N), (c) North Atlantic, (d) Northern Eurasia, (e) Chukchi Sea, (f) Canadian Arctic Archipelago (CAA), (g) Greenland; and (h) definition area.

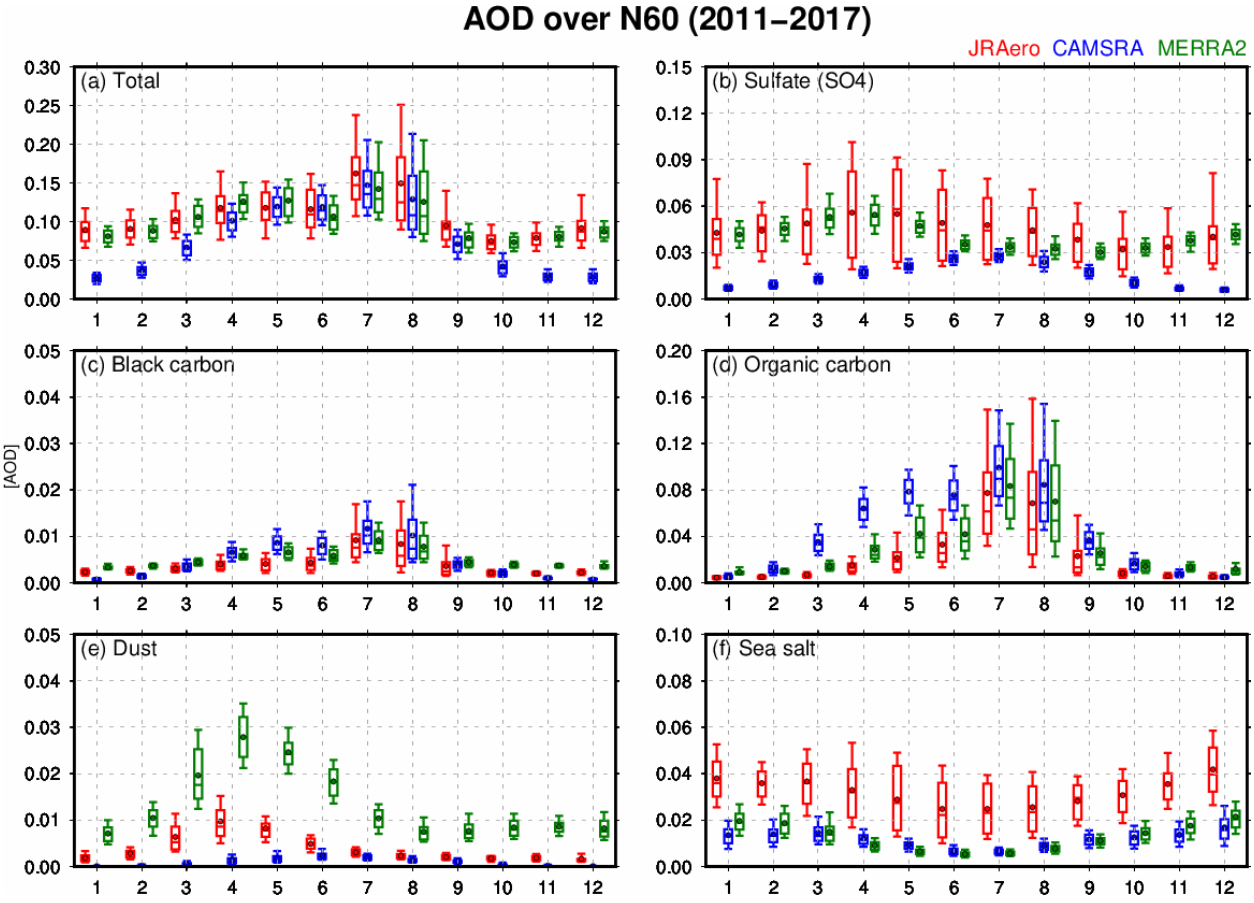

Figure 2 (a) Distribution of the six-hourly total AOD over N60 in JRAero (red), CAMSRA (blue), and MERRA-2 (green). (b–f) Distribution of the contributions of (b) sulfate, (c) black carbon, (d) organic carbon, (e) dust, and (f) sea salt aerosol to the total AOD. The circle and horizontal line in box indicate the average and median values, respectively. The range of the 25th and 75th (10th and 90th) percentile values is depicted by the box limits (vertical lines extended from the box).

The horizontal distributions of total AOD in summer showed the highest average values over Northern Eurasia (~0.3) and Northern America (~0.4) (upper panels, Fig. 3). The horizontal distributions in JRAero and MERRA2 were similar (Figs. 3a and c), while that in CAMSRA was larger in Northern Europe (Fig. 3b). The standard deviation of the total AOD in summer also depicted the largest values over Northern Eurasia and North America (lower panels, Fig. 3). The standard deviation in JRAero showed a larger value (~0.6 and ~0.5 over Northern Eurasia and Northern America, respectively) than those in CAMSRA and MERRA2 (~0.5 and ~0.4 over Northern Eurasia and Northern America, respectively). In addition, JRAero showed a large standard deviation over the Beaufort Sea, which extends toward the North Pole. A similar distribution appeared in CAMSRA and MERRA2, although its value was much smaller than that in JRAero. The standard deviation in August mainly contributed to the large standard deviation over Beaufort Sea in all the reanalyses (red contour, Fig. 3). Regarding the area of >70°N, the higher standard deviation extended from the coast of East Siberian Sea and Beaufort Sea, indicating that the high AOD airs over Northern Eurasia and Northern America were transported toward the North Pole as shown in the section 3.2. The synoptic activity over the Arctic was higher in summer (Clancy et al., 2021; Gray et al., 2021; Serreze and Barrett, 2008; Zhang et al.,

306 2004); hence, we investigate the contribution of Arctic cyclones on the Arctic AOD variability in
307 summer in the following section.

308 The representation of the reanalyses must be assessed against the observed ones, as with
309 the intercomparison of the reanalyses. Thus, although the available observations were small due
310 to cloud or surface conditions (Fig. 4c), we still calculated the correlation coefficient (Fig. 4a)
311 and the root mean square error (RMSE) (Fig. 4b) of total AODs between the reanalysis and
312 observation over the Arctic. The correlation coefficient was >0.8 over Northern Eurasia in
313 CAMSRA and MERRA2 and >0.6 in JRAero. The higher correlation coefficient corresponded to
314 CAMSRA and MERRA2 assimilating the observed AOD up to 70°N and the high latitude grids
315 with a surface albedo >0.15, respectively. By contrast, JRAero did not assimilate the observed
316 AOD at ≥60°N and, thus, the lower correlation coefficients between 60° and 70°N. The
317 correlation coefficient was ≤0.6 in JRAero and CAMSRA over the Arctic Ocean (≥70°N). Note
318 that the evaluation is independent in the north of cut-off latitude (red contour, Fig. 4c). MERRA2
319 showed higher correlation around the Barents and Kara seas. The number of available
320 observations around these areas was relatively large in MERRA2 (Fig. 4c), resulting in the
321 higher correlation in these areas.

322 The RMSE was high over Northern Eurasia in all the reanalyses (Fig. 4b). The RMSE
323 were approximately 0.3–0.4 in CAMSRA and MERRA2 and ~0.5 in JRAero. These values were
324 almost equal to the average AOD in summer (Fig. 3). The RMSE over the Arctic Ocean was
325 <0.1 in all the reanalyses, where the correlation coefficient was small. This indicates that the
326 AOD in reanalyses represented the variability well at ≤70°N, but contained errors as large as its

average value. At the higher latitude (≥70°N), the variability representation was inaccurate, and the error was smaller than the average value.

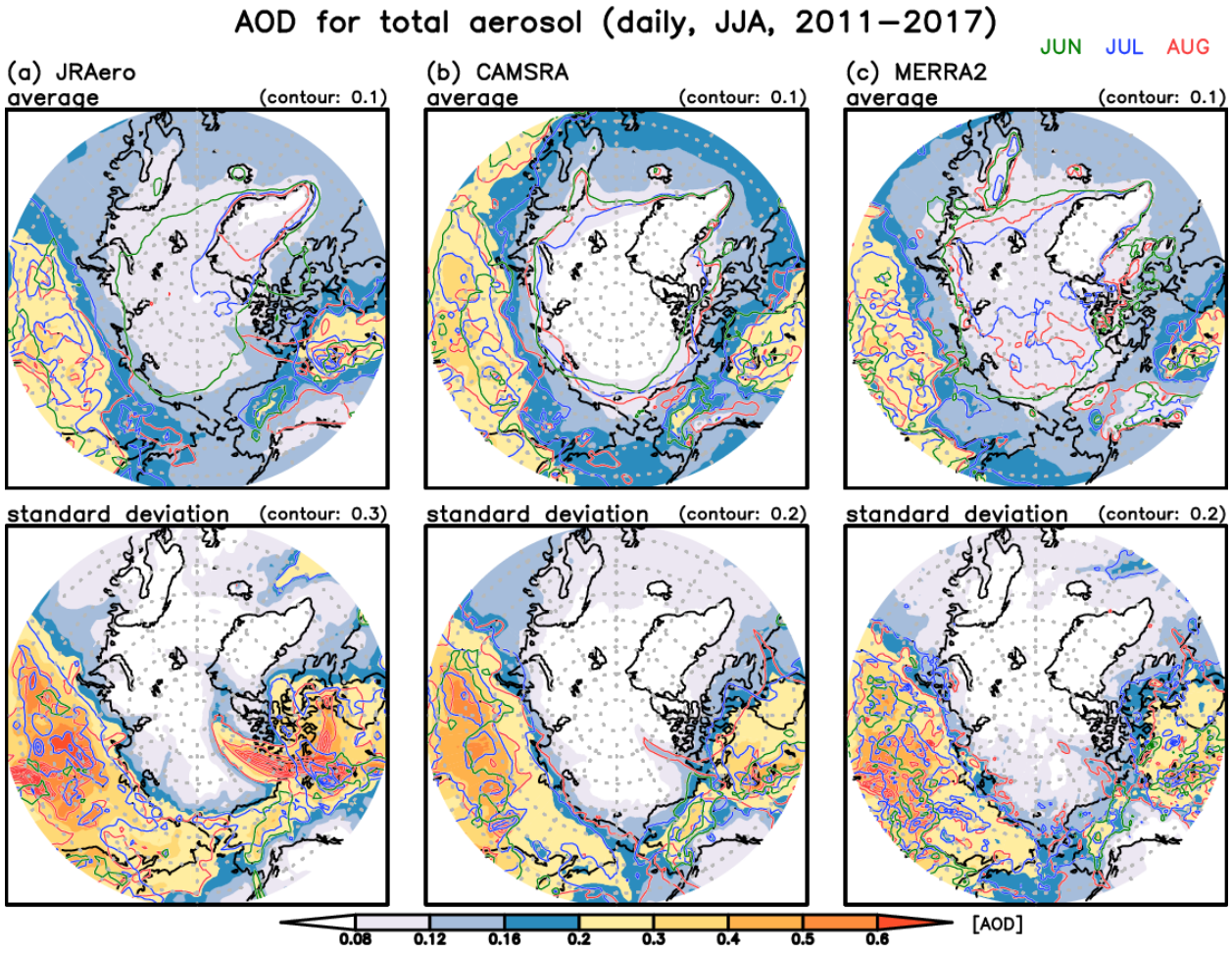

Figure 3 Average (upper) and standard deviation (lower) of the daily total AOD in (a) JRAero, (b) CAMSRA, and (c) MERRA2 in the summer of 2011–2017 (shading). These values in June, July, and

August are depicted by the green, blue, and red contours, respectively. Note that the contour interval for the standard deviation in JRAero is 0.3, while that in CAMSRA and MERRA2 is 0.2.

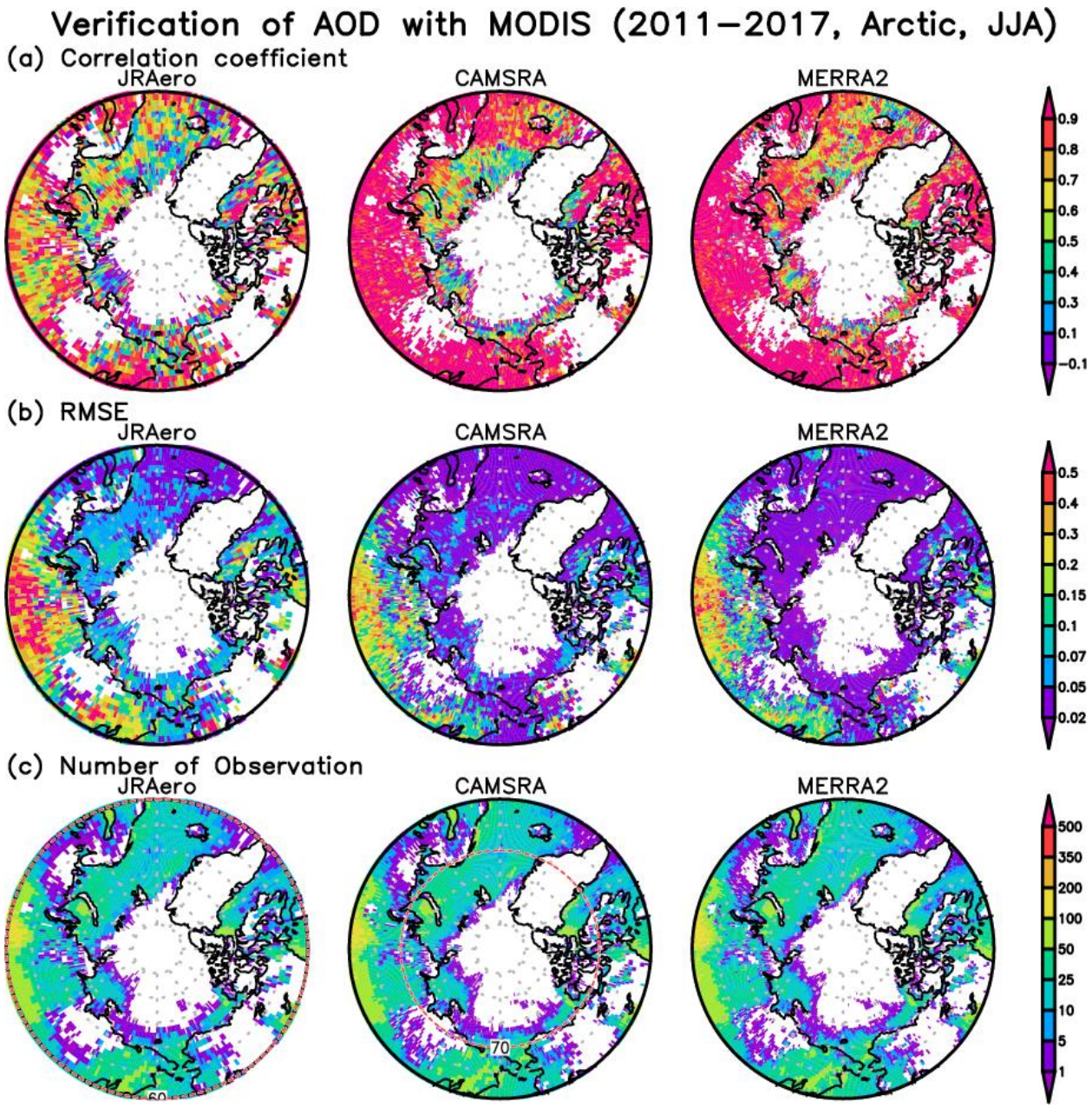

Figure 4 (a) Correlation coefficient and (b) root mean square error (RMSE) of the total AOD between the analyzed AOD in JRAero (left), CAMSRA (middle), and MERRA-2 (right) and the observed AOD by MODIS in summer (June to August) and (c) number of observations using these verifications in the

summer of 2011–2017. The cut-off latitude for the data assimilation of observed AOD was depicted by the dashed red lines in JRAero and CAMSRA in (c).

3.2 Relationship between the atmospheric circulation and the AOD in high- and low-loading days

Synoptic activities could affect the aerosol transport from Northern Eurasia and America to the Arctic Ocean. Figure 5 shows an example of the AOD variability associated with the AC in August 2012 (Simmonds and Rudeva, 2012). The AC travelled eastward and reached the Laptev Sea on 2 August 2012 (Fig. 5a). The high AOD values over Northern Eurasia was appeared in the south to south-east of the AC center. The high AOD areas were involved in the north of the AC center on 3 August (Fig. 5b). Then, the high AOD values rapidly decreased on 4 August (Fig. 5c), implying the transported aerosol removal. At the same time, another cyclone generated over Northern Eurasia and moved north-eastward. This cyclone merged with the existing AC and reached its mature stage with a central pressure of ~966 hPa at 18 UTC on 6 August 2012 (Simmonds and Rudeva, 2012). The migrating cyclone whirled up the high AOD air during the cyclogenesis, and then, the air was transported from Northern Eurasia to East Siberian Sea and Beaufort Sea along with the rim of developing cyclone (Figs. 5d and e). The high AOD area corresponded to the high standard deviation of the AOD in JRAero (Fig. 3a). The high AOD band rotated around the center with a gradual decay on 7–9 August (Figs. 5f–h). The high AOD air over Northern Eurasia was cleaned up after the AC's passing. These results indicate that the ACs play an important role in the aerosol transportation and deposition processes during its lifecycle, thereby contributing to the horizontal distribution of the average and the standard deviation of the AOD in summer (Fig. 3). In contrast, the AC in August 2016 showed a similar cyclone track and strength to that in August 2012 (Yamagami et al., 2017) without a high AOD air transport due to the lower AOD value over Northern Eurasia (Fig. S2). That is, the emission over Northern Eurasia and America are also essential in determining the aerosol variability over the Arctic.

The composite differences between the high- (upper 90th percentile values) and low- (lower 10th percentile values) loading days also indicated the influences of synoptic systems on AOD variabilities in the individual areas (Fig. 6). The AOD was high in both Northern Eurasia and America in the high-loading days over N60 (Fig. 6a), whereas the AOD difference was small over the Arctic Ocean. The difference in SLP showed a high pressure over the Pacific side of the Arctic Ocean and a low pressure over Northern Eurasia and America. The difference in emission (Fig. S3a) indicated the high AOD air formed by the high emissions over these two regions, but these airs were not transported toward the North Pole. In the high-loading days over the Arctic (Fig. 6b), high pressure existed over the Chukchi Sea, and low pressure covered the North Atlantic to the Laptev Sea, leading to the northward AOD transport. Besides, the composites difference over the central Arctic (CArctic, Fig. 3c) showed that the northward transport from the Pacific side was enhanced due to the dipole pressure pattern. Meanwhile, in the high-loading days over NEurasia (Fig. 6e), the low pressure over Northern Eurasia trapped the high AOD air. The cyclone transported the high AOD air eastward in the high-loading days over Chukchi (Fig. 6f), as depicted by the case of the AC in August 2012. The difference in the emission in Chukchi (Fig. S3f) was almost the same as that in NEurasia (Fig. S3e); thus, the difference in the AOD

between these two composites would be caused by synoptic systems. In the high-loading days over CAA (Fig. 6g), the emitted aerosol over Northern America was transported eastward. The wind associated with the high pressure over CAA and the low pressure over North Atlantic converged around the peak of the AOD difference. By contrast, the difference in SLP between the high- and low-loading days over NAtlantic showed the high pressure over the whole Arctic

Ocean; hence the transport of the high AOD air toward the Arctic Ocean was blocked over the Greenland Sea (Fig. 6d).

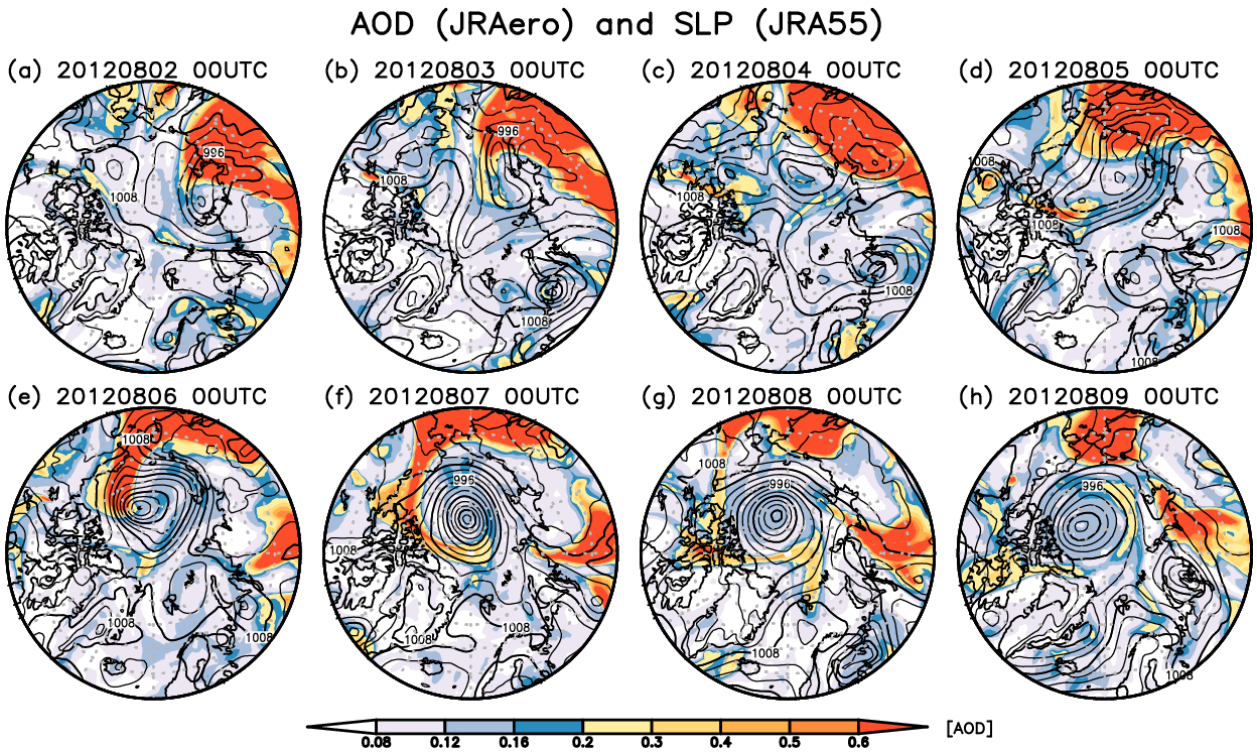

Figure 5 Example of the relationship between SLP (contour, every 4 hPa) and AOD (shaded) in the case of the great Arctic cyclone in August 2012 in a 1-day time interval at 00UTC from (a) 2 August to (h) 9 August 2012.

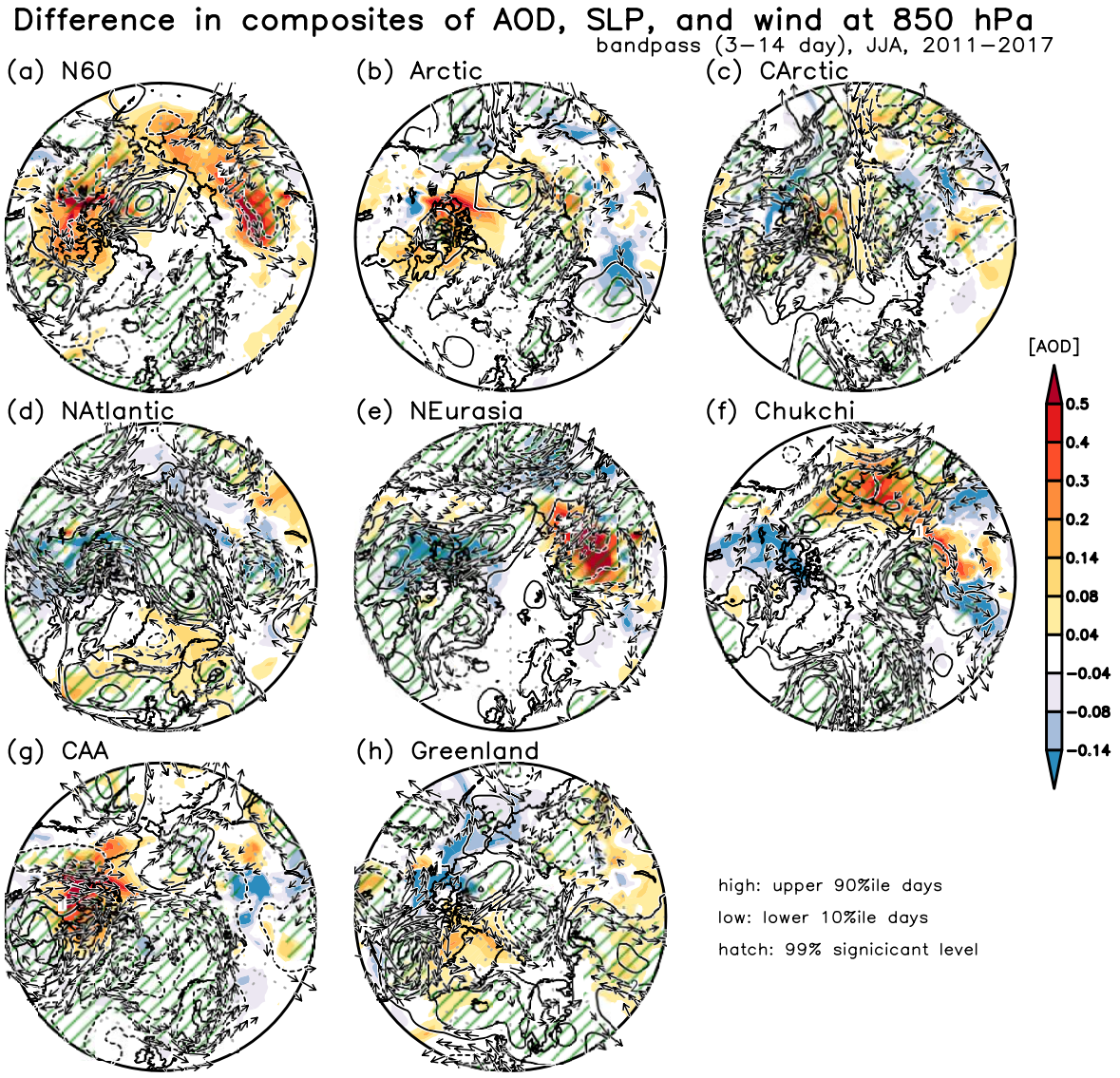

Figure 6 Difference in SLP (contour), AOD (shading), and wind at 850 hPa (vector) between the high- and low-loading days over (a) N60, (b) Arctic, (c) Central Arctic, (d) North Atlantic, (e) Northern Eurasia, (f) Chukchi, (g) CAA, and (h) Greenland. The green hatching area and the wind vectors indicate the differences in SLP and wind at a 99% statistically significant level.

3.3 EOF analysis for the AOD and relation to the atmospheric circulation

We retrieved the maximum horizontal variability by conducting an EOF analysis for the bandpass filtered AOD over N60 in the summer of 2011–2016 (Figs. 7 and 8). The structures of EOF-1 in all reanalyses exhibited the largest AOD variability over Northern Eurasia. The opposite sign of variability was observed over North America in JRAero and CAMSRA, but this was weak in MERRA2. The EOF-1 contributions to the total variability were approximately

18.0%, 13.1%, and 12.0% in JRAero, CAMSRA, and MERRA2, respectively. The PC-1 variabilities were apparent in July 2014 and 2016 (lower panels, Fig. 7), probably associated with the wildfire over Northern Eurasia (Bonder and Gorde, 2018; Tian et al., 2022). The EOF-2 also showed the dominant variabilities with opposite signs over Northern Eurasia (upper panels, Fig. 8). The contributions of EOF-2 in JRAero, CAMSRA, and MERRA2 were 8.5%, 11.4%, and 11.5%, respectively. In addition to July 2014 and 2016, remarkable variabilities were found in both PC-1 and -2 from the end of July to early August 2012 (dark blue line in lower panels in Figs. 7 and 8), which is possibly associated with the AC in August 2012 (Fig. 5).

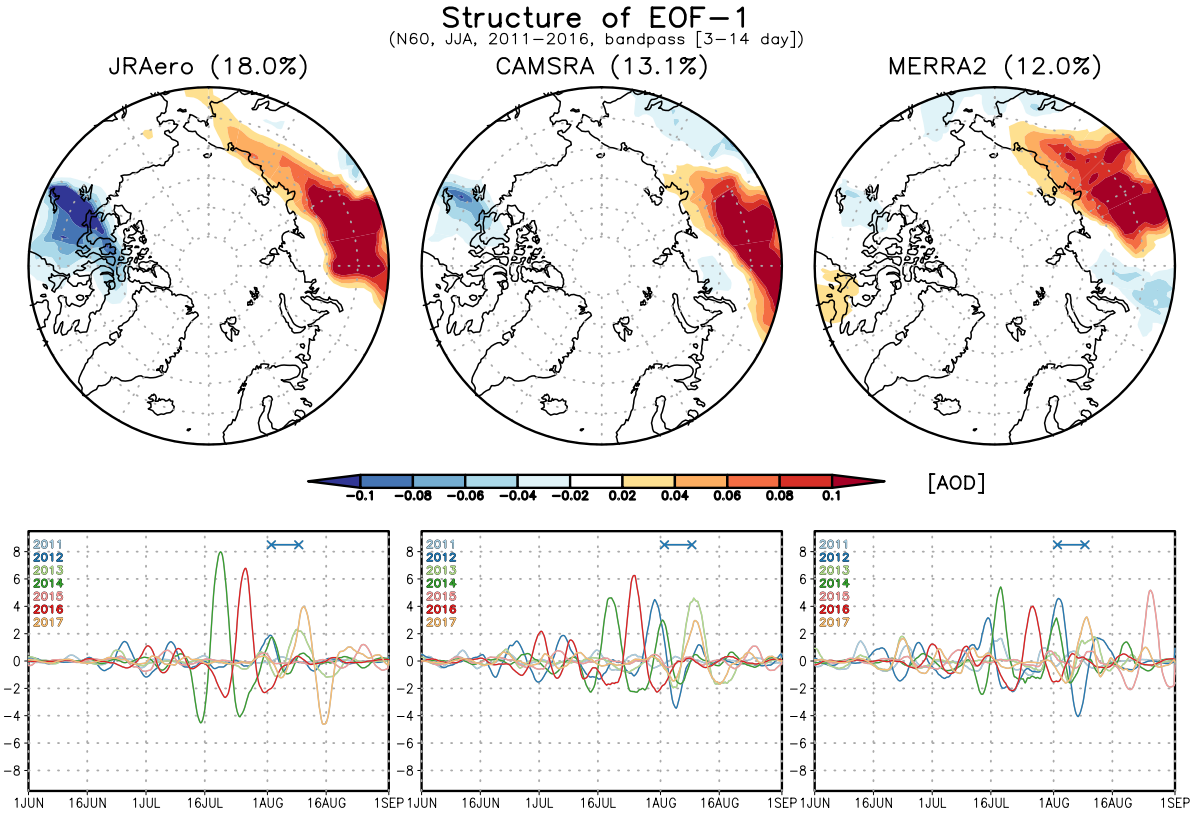

Figure 7 (Upper) Horizontal structure of the 3–14-day running averaged AOD for EOF-1 and (lower) the time series of PC-1 in (left) JRAero, (center) CAMSRA, and (right) MERRA2 in the summer of 2011–

2016. Dark blue lines with crosses in lower panels represent the period for the AC in August 2012 in Fig.5.

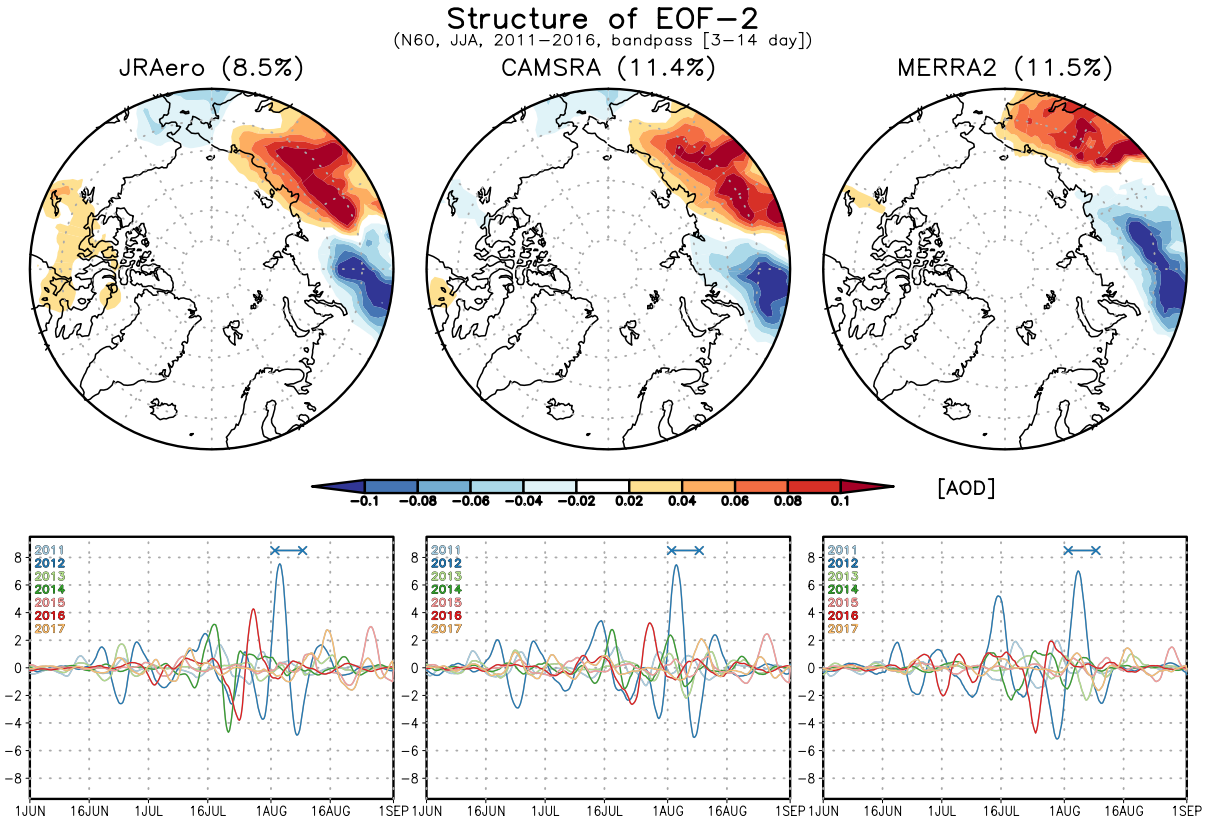

Figure 8 Similar to Fig.7, but for EOF-2.

The lag regression analysis showed the AOD transport associated with PC-1 and PC-2. At a 0-day lag, the regressed AOD was almost similar to the EOF-1 and EOF-2 structures (third column, Fig. 9; upper panels, Figs. 7 and 8). The AOD regressed onto PC-1 showed a positive values over northeast Eurasia in all the reanalyses at the −3-day lag. The positive AOD moved north-eastward, reaching the Chukchi Sea to Alaska at a +5-day lag (Figs. 9a–c). The regressed SLP onto PC-1 in JRAero and CAMSRA (Figs. 9a and b) showed a small low-pressure anomaly over the Laptev Sea at the −3-day lag, while a high-pressure anomaly existed over the Pacific side of the Arctic Ocean. The low-pressure anomaly persisted over the same area up to +1-day lag. Another low-pressure anomaly appeared at −3-day lag over Northern Eurasia, where the regressed AOD was positive. The low-pressure anomaly at lower latitudes gradually developed and moved north-eastward with the positive AOD, indicating that the low-pressure anomaly trapped and transported the aerosol. In MERRA2 (Fig. 9c), the low-pressure anomaly over Northern Eurasia extended to the Laptev Sea at −3-day lag. All the reanalyses showed that

positive AOD area was transported from the lower to higher latitudes through the two low-pressure anomalies around the +1–3-day lag. The positive AOD inside the merged low-pressure anomaly disappeared at +3 to 5-day lag, indicating the removal of the aerosol. The regressed AOD over Eurasia was negative after the low-pressure anomaly passed.

The SLP regressed onto PC-2 showed that the low-pressure anomaly over Northern Eurasia extended to the Arctic Ocean in all the reanalyses at −3-day lag (Figs. 9d–f), which contained the positive AOD region on its south–southeast side. The low-pressure anomaly transported the positive AOD north-eastward from the −3 to +1-day lag. After the +3-day lag, the positive AOD area inside the low-pressure anomaly disappeared and reached Northern Pacific to Alaska outside of the low pressure. As with PC-1, the AOD over Northern Eurasia was negative after the low-pressure anomaly passed.

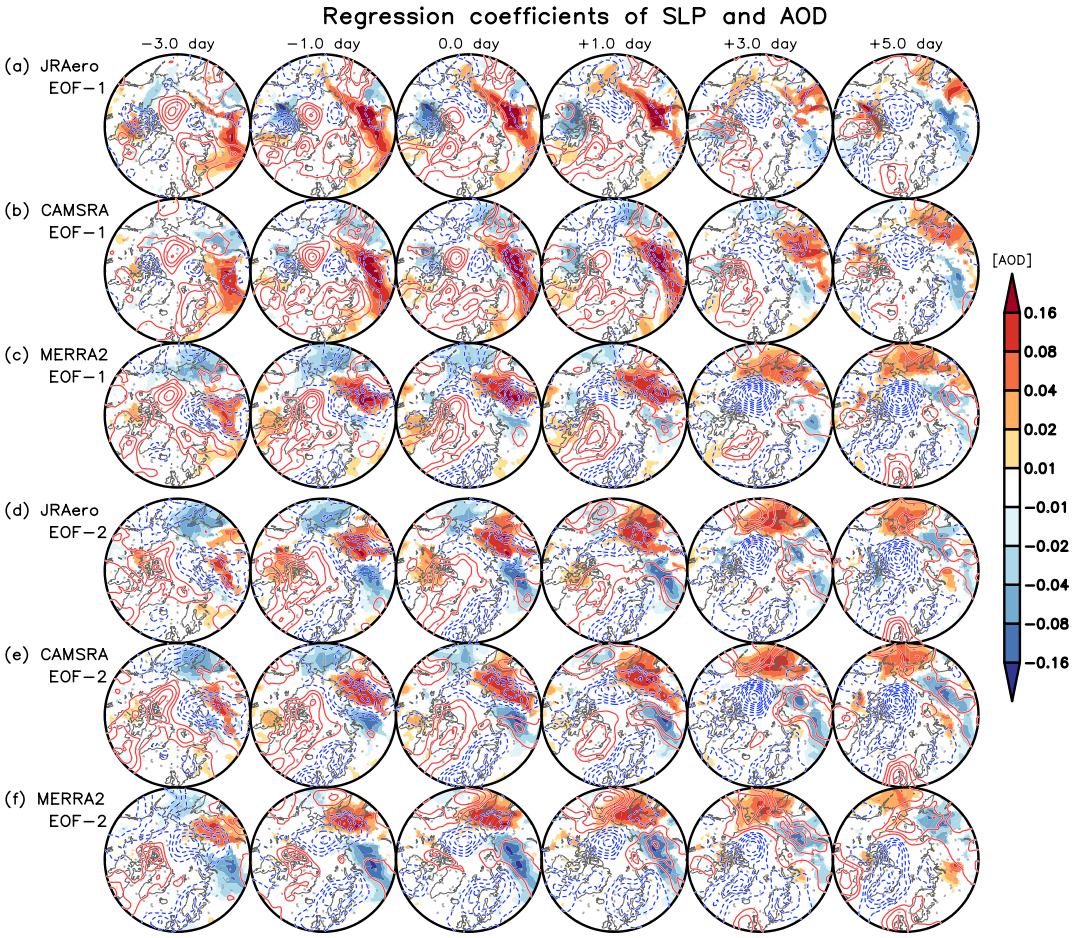

Figure 9 Total AOD (shading) regressed onto (a–c) PC-1 and (d–f) PC-2 in (a, d) JRAero, (b, e) CAMSRA, and (c, f) MERRA2. The regression coefficients with a 95% significant level from the −3 to

+5-day lag were plotted in two-day interval and 0-day lag. The blue (positive) and red (negative) contours show the SLP in JRA-55 regressed onto EOF-1 and EOF-2 in each aerosol reanalysis.

3.4 The OC and SS aerosol variability associated with the atmospheric circulation

In terms of environmental impacts of aerosol species, sulfate (high cloud condensation nucleation activity and acidification), BC (light absorption), and mineral dust (light absorption and ice nucleation activity) have been focused on. On the other hand, OC mainly contributed to the total AOD variability associated with EOF-1 and -2 in all reanalyses (Figs. S1 and S4). Besides, recent studies observed the high concentration of biogenic aerosols due to oceanic sources over the Arctic (Inoue et al., 2021; Poter et al., 2021). Thus, we focused on the relationship between OC and SS in reanalyses and atmospheric circulation in this section.

For the regressed OC deposition fluxes onto PC-1 (Figs. 10a and b), the wet deposition was dominant over the dry deposition. The wet deposition flux was positive from the south of the high-latitude low-pressure anomaly to the east of the low-latitude low-pressure anomaly at the −3-day lag. At the −1–0-day lag, the wet deposition was enhanced over Northern Eurasia, where the positive AOD appeared. While the wet deposition flux gradually decreased at the 0 to +5-day lag over Northern Eurasia, the positive wet deposition flux increased over Alaska at the +1 to +3-day lag. These results suggested that most of OC aerosol was removed by the wet deposition processes over Northern Eurasia, but some parts reached Alaska. The deposition occurred from the southern to south-eastern side of the merged low-pressure anomaly. Although the SS deposition fluxes regressed onto PC-1 showed positive values around the low-pressure anomaly over the Laptev Sea at −3 to −1-day lag, the fluxes disappeared and no remarkable signal was observed over the Arctic region at 0 to +5-day lag (Figs. 10c and d).

The deposition fluxes regressed onto PC-2 again depicted that the wet deposition was much larger than the dry deposition (Figs. 11a and b). As with the regression onto PC-1, the positive wet deposition flux appeared over Northern Eurasia at the −3 to +1-day lag, indicating that OC aerosol was removed during the transport. In contrast to that in PC-1, the positive flux appeared inside the low-pressure anomaly over Northern Eurasia at these times. At the +1 to +3-day lag, the low-pressure anomaly reached the Pacific side of the Arctic Ocean, and the positive wet deposition appeared south of the low-pressure anomaly center. The positive wet deposition also occurred over the Sea of Okhotsk and Alaska at the +3–5-day lag. At these lags, the positive deposition flux regressed onto PC-2 reached further high latitude compared with that regressed onto PC-1, suggesting that the aerosol variability associated with EOF-2 influences the Arctic climate systems.

In addition to OC, the deposition flux of SS also showed a significant positive value around the south of the low-pressure anomaly center at the +1 to +3-day lag (Figs. 11c and d). These results suggested that the surface wind due to the low-pressure anomaly induced the SS aerosol emission. Subsequently, SS aerosol could be removed by low-level clouds and the precipitation associated with the low-pressure anomaly (i.e., in-cloud scavenging and below-cloud scavenging, respectively) around the MIZ. Considering that the higher SS contribution in JRAero (Figs. 2f and S1e) and no significant deposition flux of SS aerosol in MERRA2 (Figs.

S5c and d and S6c and d), further analyses are required to reveal whether or not the NWP models can represent these local processes. In contrast, the regressed deposition fluxes of OC aerosol in MERRA2 (Figs. S5a and b and S6a and b) consistent with those in JRAero. Therefore, the consisstency of the OC aerosol behavior associated with EOF-1 and EOF-2 variabilities PC-1 and PC-2 might be relatively high among the reanalyses.

Cloud cover, relative humidity (RH), and precipitation play an essential role in the wet removal processes. The regressed total cloud cover (TCC) onto PC-2 increased with the development of the low-pressure anomaly at the −3–0-day lag (Fig. 12a), especially around the southern part of the low-pressure anomaly. Although the positive TCC separated from the low-pressure anomaly when the anomaly reached the Arctic Ocean, the coefficient again increased inside the low-pressure anomaly at the +1 to +3-day lag. The positive TCC persisted up to the +5-day lag. The regressed low-level cloud cover (LCC) was almost similar to the TCC (Fig. 12b), indicating that the LCC dominated the TCC variability associated with PC-2. The RH at 850 hPa (RH850) regression also illustrated a similar horizontal distribution to the TCC and the LCC. The PC-2 variability (up to ~8) and the regression coefficient of RH850 (≥2.5%) indicated the variability of RH850 was as much as 20% around the low-pressure anomaly at the +1–3-day lag. In JRAero, 80% and 20% OC were emitted as hydrophobic and hygroscopic states, respectively, and the hydrophobic OC also changed to a hygroscopic state during the 1.2-day e-folding time (Yumimoto et al., 2017). Therefore, most of the OC emitted over Northern Eurasia changed into the hygroscopic state during transport and removed by the wet processes associated with the low-pressure anomaly. The regressed total precipitation (Fig. 12d) suggested that both in- and below-cloud scavenging could contribute to the wet deposition of OC inside the low-pressure anomaly. These results showed that the aerosol variabilities (i.e., transportation, aging,

and removal) over the Arctic were mostly controlled by the AC generation, development, and associated cloud and precipitation.

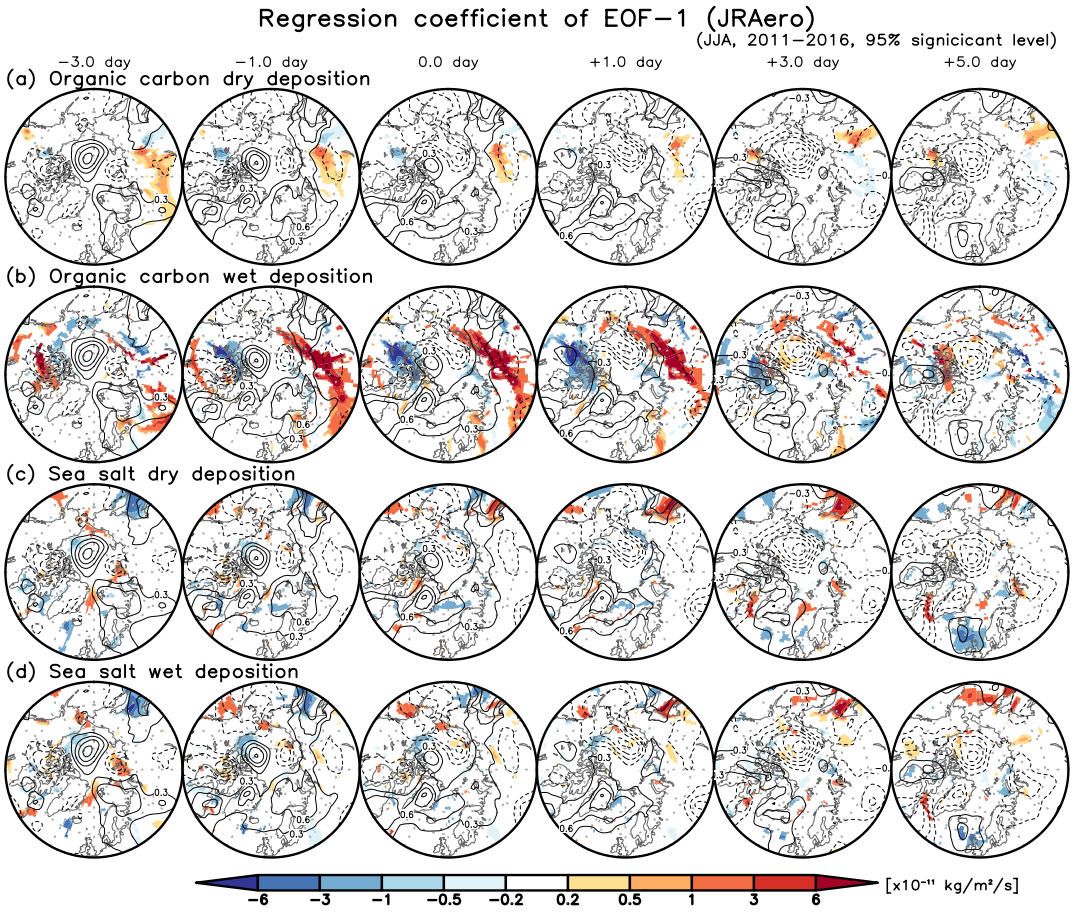

Figure 10 Similar to Figs. 9a, but for the (a, c) dry and (b, d) wet deposition fluxes of (a, b) organic carbon and (c, d) sea salt with 95% significant level in JRAero. The regression coefficient with a 95% significant level is plotted.

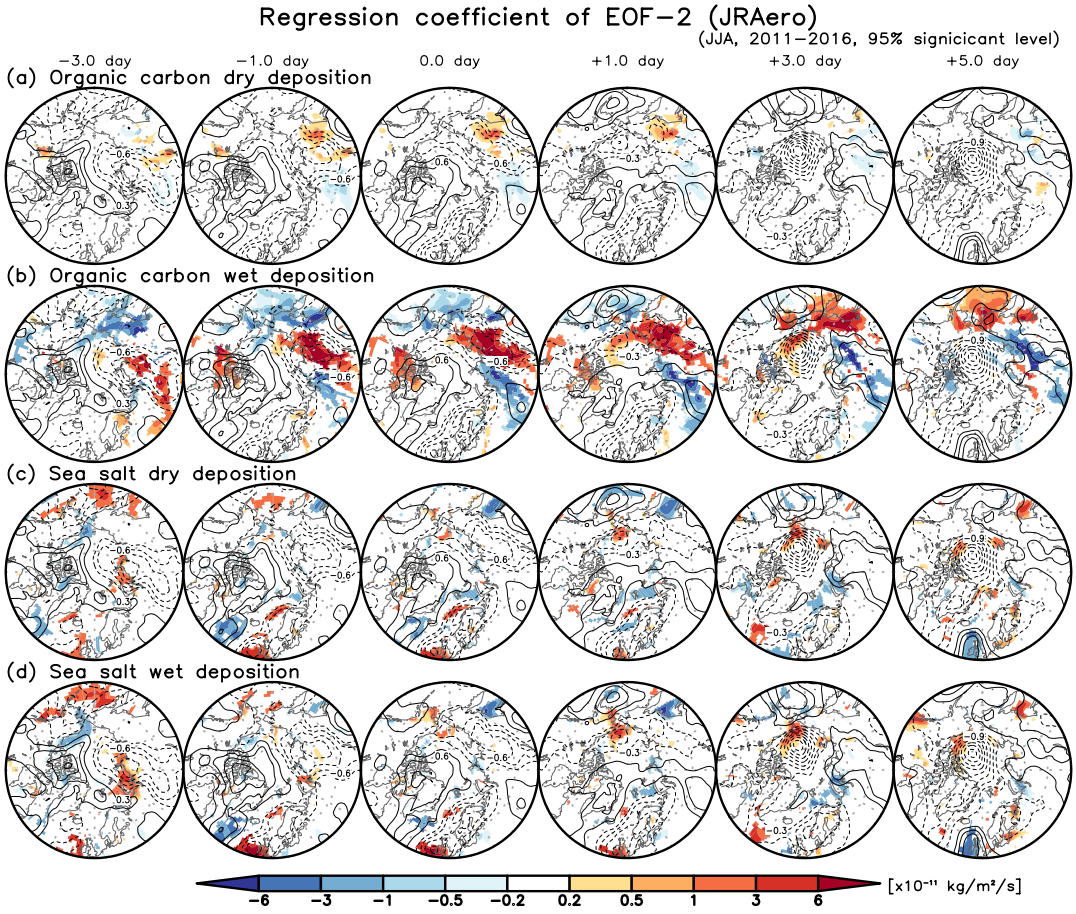

Figure 11 Similar to Fig. 10, but for PC-2.

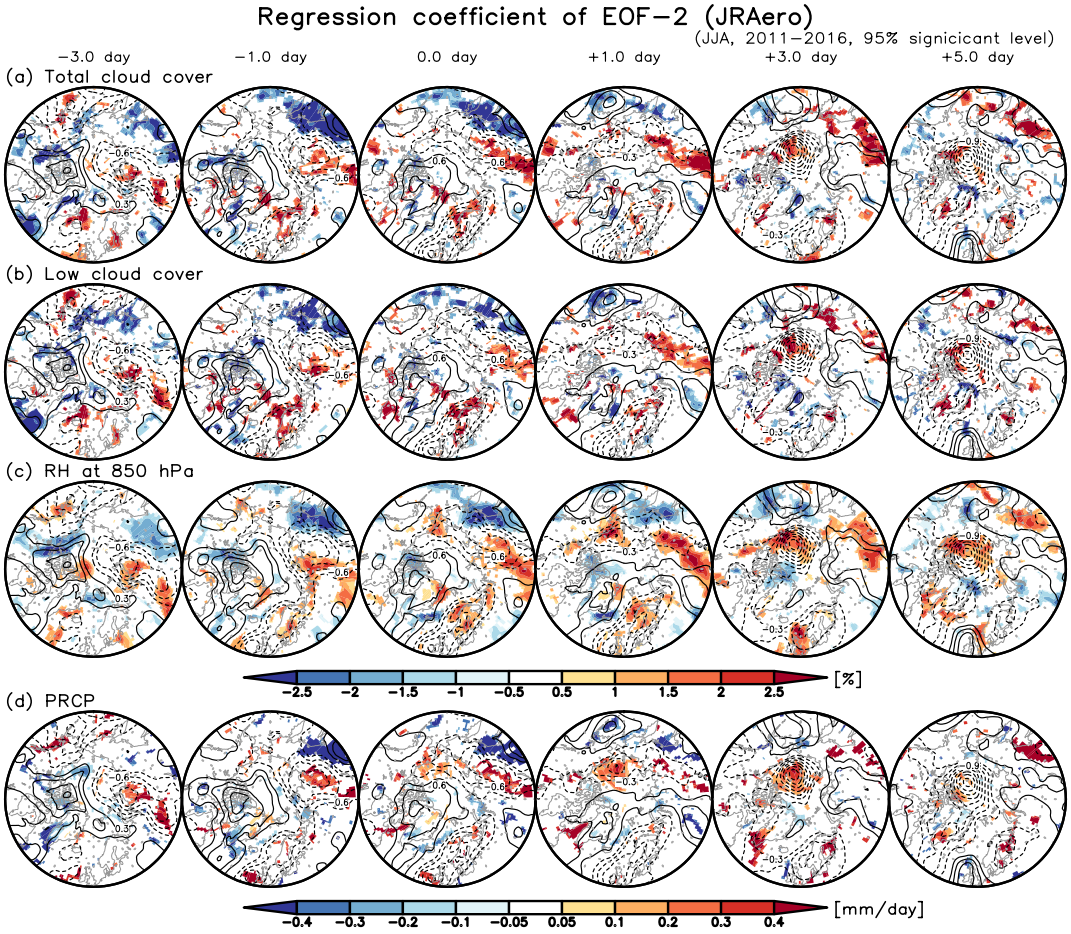

Figure 12 Similar to Figs. 8d–f, but for the (a) total cloud cover, (b) low-level cloud cover, (c) relative humidity at 850 hPa, and (d) precipitation in JRA-55. The regression coefficient with a 95% significant level is plotted.

4 Conclusions

This study evaluated the Arctic aerosol representation among three reanalyses, namely JRAero, CAMSRA, and MERRA2, in terms of the AOD. In particular, the summertime Arctic aerosol variability caused by the synoptic-scale atmospheric circulation was investigated herein.

In JRAero, the monthly climatological variability of the total AOD showed the highest values in July and August over the north of 60°N (N60), Northern Eurasia (NEurasia), and Chukchi and in August over the CAA and the Arctic (north of 70°N). These climatological AOD variabilities suggested that the high AOD over NEurasia, Chukchi, and CAA contributed to the high AOD over N60. The aerosol emitted over NEurasia and CAA would reach the higher latitude and create a peak in August over the Arctic, which is consistent with the findings of previous studies (e.g., Garrett et al., 2010, 2011; Stohl, 2006, Schmale et al., 2022; Stohl et al., 2007). The monthly variability was small over North Atlantic and Greenland.

The histogram of the six-hourly total AOD over the N60 showed an almost similar distribution among the reanalyses from April to September. These results were consistent with those of Xian et al. (2022), who compared the monthly AOD variabilities in CAMSRA, MERRA2, and NAPPS-RA. JRAero represented relatively high AOD events compared to CAMSRA and MERRA2 in summer. The AOD in CAMSRA was generally smaller than those in JRAero and MERRA2 from October to March.

In spring and summer, although the total AOD from the three reanalyses was at a similar level, the contributions of the individual aerosol species to the total AOD remarkably differed among the reanalyses. In term of contribution of aerosol species on the total AOD, OC showed the largest contribution to the total AOD in spring and summer in all reanalyses (~10–70%). Besides, the average values and variabilities of OC were almost similar among the reanalyses in the peak months, July and August. The second largest contribution was made by sulfate in the three reanalyses (~20–60%) in the two months. However, JRAero exhibited a contribution of SS as large as that of sulfate. Also, dust (OC) aerosol showed a larger contribution in MERRA2 (CAMSRA) compared to JRAero and CAMSRA (JRAero and MERRA2) from March to June. As mentioned by Flemming et al. (2017), the decrease in a certain aerosol contribution was compensated for by an increase in another aerosol contribution because the data assimilation bound the total AOD in the reanalysis. Thus, these differences among the reanalyses reflected the uncertainties of aerosol processes among the CTMs. The model uncertainties would be more apparent over the high Arctic because the available observations are limited.

The horizontal distribution of the average total AOD was similar among the reanalyses. In all reanalyses, the larger AOD appeared over Northern Eurasia, Alaska, and CAA. The standard deviation of AOD in JRAero was larger over these regions than in CAMSRA and MERRA2, especially over the CAA to the Beaufort Sea in August. Compared to limited satellite observations, the total AOD variability was generally represented up to 75°N ($R \geq 0.6$) in all the reanalyses. However, these reanalyses contained errors as large as the average total AOD (RMSE: ~0.3–0.5), suggesting that CTMs have some difficulty in predicting the magnitude of the total AOD and the aerosol composition with very limited observations over the Arctic. Thus,

we need careful treatment when using individual aerosol species and/or the magnitude of the total AOD provided by aerosol reanalyses over the Arctic.

The EOF analysis was applied to the summertime total AOD over N60 on the synoptic timescales. EOF-1 had the largest variability over central Northern Eurasia, while EOF-2 depicted large variabilities in both eastern and western Northern Eurasia with opposite signs. The SLP distributions regressed onto PC-1 and -2 showed that positive AOD anomalies are associated with the generation, traveling, and development of low-pressure anomalies. Regarding EOF-1 variability in JRAero and CAMSRA, a low-pressure anomaly existed over the Kara Sea at the −3-day lag. At the same time, another low-pressure anomaly developed over Northern Eurasia. These two anomalies gradually approached each other and merged over the Pacific side of the Arctic Ocean at the −3–0.0-day lag. The positive AOD values over Northern Eurasia were transported northward by the low-pressure anomaly and were handed over to the other low-pressure anomaly during the merging at the +1–3-day lag. The regression onto PC-2 also showed that the low-pressure anomaly transported the positive AOD area over Northern Eurasia during its development, albeit having no pre-existing low-pressure anomaly over the Arctic Ocean. In both EOF-1 and -2 cases, low-pressure anomalies played an essential role in removing the aerosols by the associated cloud and precipitation. EOF-2 was particularly related to the positive deposition fluxes of OC (the main contributor to the total AOD) and SS over the Chukchi Sea, suggesting that aerosol influences the Arctic climate systems (e.g., sea ice and snow) (Niwano et al., 2021).

The abovementioned results indicate that the Arctic aerosol variability on the synoptic timescales is significantly related to the AC generation and development in terms of transport, aging, and deposition. Hence, the aerosol atmospheric river (Chakraborty et al., 2021) at high latitudes could be formed by the ACs. At the present time, an accurate medium-range AC prediction is one of the difficulties faced by NWP models (Caupte and Torn, 2021; Yamagami et al., 2018a, b, 2019; Yamagami and Matsueda, 2021). The forecast error associated with the ACs could lead to errors in the aerosol prediction over the Arctic. Yamashita et al. (2021) demonstrated that the use of higher horizontal resolution of an NWP model results in the better BC aerosol prediction in the middle- to upper-level troposphere due to the sharpened vertical motions associated with a mid-latitude cyclone. By contrast, although the aerosol reanalysis was made using the atmospheric fields from an operational analysis or reanalysis, the aerosol fields contained significant uncertainties over the Arctic. Thus, even with accurate atmospheric fields, CTMs could lead to aerosol prediction errors due to the insufficient representation of the chemical processes. Flemming et al. (2017) demonstrated that the total AOD showed better representation in CAMSiRA over the globe, except over Southeast Asia, than in MACCRA due to the update of the prediction system (i.e., NWP model, CTM, and assimilation system), even though CAMSiRA used a lower-resolution model. Kajino et al. (2019b) also showed large uncertainties of both chemical processes in CTMs, especially through in-cloud scavenging, and the background atmospheric fields. Further observational studies would progress our understanding of the atmosphere–chemistry interactions, which improvs the aerosol processes

represented in CTMs and reduce the uncertainties. It would enhance aerosol prediction and give feedback to weather and climate predictions.

Acknowledgments

The authors thank the MRI and Kyusyu University, ECMWF, and NASA GMAO for providing the JRAero, CAMSRA, and MERRA-2, respectively. The authors also thank the MRI/JMA for providing the JRA55 reanalysis datasets. The authors are grateful to Prof. K. Yumimoto at Kyusyu University for allowing us to use the formatted MODIS AOD datasets. This study was mainly supported by the Japanese Society for the Promotion of Sciences (JSPS) KAKENHI grant no. JP22J01703, and partly supported by the Arctic Challenge for Sustainability II (ArCS II), Grant Number JPMXD1420318865.

Open Research

The JRAero dataset can be obtained upon data request from the developers (https://www.riam.kyushu-u.ac.jp/taikai/JRAero/index.html). The CAMSRA and MERRA-2 aerosol reanalyses are available at the Atmosphere Data Store (ADS) on the Copernicus Atmosphere Monitoring Service (CAMS; https://ads.atmosphere.copernicus.eu/cdsapp#!/home) and the MERRA2 webpage on NASA GMAO (https://gmao.gsfc.nasa.gov/reanalysis/MERRA-2/). The JRA-55 reanalysis is available at JRA-55 webpage (https://jra.kishou.go.jp/JRA-55/index_ja.html).

References

Aizawa, T., Ishii, M., Oshima, N., Yukimoto, S., & Hasumi, H. (2021). Arctic Warming and Associated Sea Ice Reduction in the Early 20th Century Induced by Natural Forcings in MRI-ESM2.0 Climate Simulations and Multimodel Analyses. Geophysical Research Letters, 48(8), 1–10. https://doi.org/10.1029/2020GL092336

636 Benedetti, A., Morcrette, J. J., Boucher, O., Dethof, A., Engelen, R. J., Fisher, M., Flentje, H.,
637 Huneeus, N., Jones, L., Kaiser, J. W., Kinne, S., Mangold, A., Razinger, M., Simmons, A. J.,
638 & Suttie, M. (2009). Aerosol analysis and forecast in the European Centre for Medium-
639 Range Weather Forecasts integrated forecast system: 2. data assimilation. *Journal of*
640 *Geophysical Research Atmospheres*, *114*(13). https://doi.org/10.1029/2008JD011115
641 Benedetti, A., & Vitart, F. (2018). Can the direct effect of aerosols improve subseasonal
642 predictability? *Monthly Weather Review*, *146*(10), 3481–3498.
643 https://doi.org/10.1175/MWR-D-17-0282.1
644 Bhattacharjee, P. S., Wang, J., Lu, C., & Tallapragada, V. (2018). The implementation of NEMS
645 GFS Aerosol Component (NGAC) Version 2.0 for global multispecies forecasting at
646 NOAA/NCEP – Part 2: Evaluation of aerosol optical thickness. *Geoscientific Model*
647 *Development*, *11*(6), 2333–2351. https://doi.org/10.5194/gmd-11-2333-2018
648 Bondur, V. G., & Gordo, K. A. (2018). Satellite Monitoring of Burnt-out Areas and Emissions of
649 Harmful Contaminants Due to Forest and Other Wildfires in Russia. *Izvestiya - Atmospheric*
650 *and Ocean Physics*, *54*(9), 955–965. https://doi.org/10.1134/S0001433818090104
651 Bossioli, E., Sotiropoulou, G., Methymaki, G., & Tombrou, M. (2021). Modeling Extreme
652 Warm-Air Advection in the Arctic During Summer: The Effect of Mid-Latitude Pollution
653 Inflow on Cloud Properties. Journal of Geophysical Research: Atmospheres, 126(7).
654 https://doi.org/10.1029/2020JD033291
655 Bozzo, A., Benedetti, A., Flemming, J., Kipling, Z., & Rémy, S. (2020). An aerosol climatology
656 for global models based on the tropospheric aerosol scheme in the Integrated Forecasting
657 System of ECMWF. *Geoscientific Model Development*, *13*(3), 1007–1034.
658 https://doi.org/10.5194/gmd-13-1007-2020

Buchard, V., Randles, C. A., da Silva, A. M., Darmenov, A., Colarco, P. R., Govindaraju, R., … Yu, H. (2017). The MERRA-2 aerosol reanalysis, 1980 onward. Part II: Evaluation and case studies [Dataset]. *Journal of Climate*, 30(17), 6851–6872. https://doi.org/10.1175/JCLI-D-16-0613.1

Gong, S. L., Lavoué, D., Zhao, T. L., Huang, P., & Kaminski, J. W. (2012). GEM-AQ/EC, an on-line global multi-scale chemical weather modelling system: model development and evaluation of global aerosol climatology. *Atmospheric Chemistry and Physics*, *12*(17), 8237–8256. https://doi.org/10.5194/acp-12-8237-2012

Chakraborty, S., Guan, B., Waliser, D. E., da Silva, A. M., Uluatam, S., & Hess, P. (2021). Extending the Atmospheric River Concept to Aerosols: Climate and Air Quality Impacts. Geophysical Research Letters, 48(9). https://doi.org/10.1029/2020GL091827

Chin, M., Ginoux, P., Kinne, S., Torres, O., Holben, B. N., Duncan, B. N., … Nakajima, T. (2002). Tropospheric aerosol optical thickness from the GOCART model and comparisons with satellite and sun photometer measurements. Journal of the Atmospheric Sciences, 59(3 PT 1), 461–483. https://doi.org/10.1175/1520-0469(2002)059<0461:taotft>2.0.co;2

Clancy, R., Bitz, C. M., Blanchard-Wrigglesworth, E., McGraw, M. C., & Cavallo, S. M. (2021). A cyclone-centered perspective on the drivers of asymmetric patterns in the atmosphere and sea ice during Arctic cyclones. Journal of Climate, 1–47. https://doi.org/10.1175/jcli-d-21-0093.1

Colarco, P., A. da Silva, M. Chin, and T. Diehl, 2010: Online simulations of global aerosol distributions in the NASA GEOS-4 model and comparisons to satellite and ground-based aerosol optical depth. *J. Geophys. Res.*, 115, D14207, doi:10.1029/2009JD012820

Crawford, A. D., & Serreze, M. C. (2016). Does the summer Arctic frontal zone influence arctic ocean cyclone activity? *Journal of Climate*, 29(13), 4977–4993. https://doi.org/10.1175/JCLI-D-15-0755.1

Creamean, J. M., de Boer, G., Telg, H., Mei, F., Dexheimer, D., Shupe, M. D., … McComiskey, A. (2021). Assessing the vertical structure of Arctic aerosols using balloon-borne measurements. *Atmospheric Chemistry and Physics*, *21*(3), 1737–1757. https://doi.org/10.5194/acp-21-1737-2021

DeRepentigny, P., Jahn, A., Holland, M. M., Kay, J. E., Fasullo, J., Lamarque, J.-F., … Barrett, A. P. (2022). Enhanced simulated early 21st century Arctic sea ice loss due to CMIP6 biomass burning emissions. *Science Advances*, *8*(30), 2405. https://doi.org/10.1126/SCIADV.ABO2405

Flemming, J., Huijnen, V., Arteta, J., Bechtold, P., Beljaars, A., Blechschmidt, A.-M., … Tsikerdekis, A. (2015). Tropospheric chemistry in the Integrated Forecasting System of ECMWF. *Geoscientific Model Development*, *8*(4), 975–1003. https://doi.org/10.5194/gmd-8-975-2015

Flemming, J., Benedetti, A., Inness, A., Engelen J, R., Jones, L., Huijnen, V., … Katragkou, E. (2017). The CAMS interim Reanalysis of Carbon Monoxide, Ozone and Aerosol for 2003-2015. *Atmospheric Chemistry and Physics*, *17*(3), 1945–1983. https://doi.org/10.5194/acp-17-1945-2017

Garrett, T., Zhao, C., & Novelli, P. (2010). Assessing the relative contributions of transport efficiency and scavenging to seasonal variability in Arctic aerosol. *Tellus B: Chemical and Physical Meteorology*, *62*(3), 190–196. https://doi.org/10.1111/j.1600-0889.2010.00453.x

Garrett, T. J., Brattström, S., Sharma, S., Worthy, D. E. J., & Novelli, P. (2011). The role of scavenging in the seasonal transport of black carbon and sulfate to the Arctic. *Geophysical Research Letters*, *38*(16). https://doi.org/10.1029/2011GL048221

Gelaro, R., McCarty, W., Suárez, M. J., Todling, R., Molod, A., Takacs, L., … Zhao, B. (2017). The Modern-Era Retrospective Analysis for Research and Applications, Version 2 (MERRA-2) [Dataset]. *Journal of Climate*, *30*(14), 5419–5454. https://doi.org/10.1175/JCLI-D-16-0758.1

Gong, S. L., Lavoué, D., Zhao, T. L., Huang, P., & Kaminski, J. W. (2012). GEM-AQ/EC, an on-line global multi-scale chemical weather modelling system: model development and evaluation of global aerosol climatology. *Atmospheric Chemistry and Physics*, *12*(17), 8237–8256. https://doi.org/10.5194/acp-12-8237-2012

Gray, S. L., Hodges, K. I., Vautrey, J. L., & Methven, J. (2021). The role of tropopause polar vortices in the intensification of summer Arctic cyclones. Weather and Climate Dynamics, 2(4), 1303–1324. https://doi.org/10.5194/wcd-2-1303-2021

Grell, G. A., S. E. Peckham, R. Schmitz, S. A. McKeen, G. Frost, W. C. Skamarock, and B. Eder, (2005) Fully coupled “online” chemistry within the WRF model. Atmos. Environ., 39, 6957–6975. https://doi.org/10.1016/j.atmosenv.2005.04.027

Haywood, J., & Boucher, O. (2000). Estimates of the direct and indirect radiative forcing due to tropospheric aerosols: A review. *Reviews of Geophysics*, *38*(4), 513–543. https://doi.org/10.1029/1999RG000078

Hersbach, H., Bell, B., Berrisford, P., Hirahara, S., Horányi, A., Muñoz-Sabater, J., … Thépaut, J. (2020). The ERA5 global reanalysis. Quarterly Journal of the Royal Meteorological Society, 146(730), 1999–2049. https://doi.org/10.1002/qj.3803

Heidinger, A. K., Foster, M. J., Walther, A., & Zhao, X. (2014). The Pathfinder Atmospheres–Extended AVHRR climate dataset. *Bull. Amer. Meteor. Soc.*, 95, 909–922, doi:10.1175/BAMS-D-12-00246.1.

Huang, X., & Ding, A. (2021). Aerosol as a critical factor causing forecast biases of air temperature in global numerical weather prediction models. *Science Bulletin*, *66*(18), 1917–1924. https://doi.org/10.1016/j.scib.2021.05.009

Im, U., Tsigaridis, K., Faluvegi, G., Langen, P. L., French, J. P., Mahmood, R., … Brandt, J. (2021). Present and future aerosol impacts on Arctic climate change in the GISS-E2.1 Earth system model. *Atmospheric Chemistry and Physics*, *21*(13), 10413–10438. https://doi.org/10.5194/acp-21-10413-2021

Inness, A., Ades, M., Agustí-Panareda, A., Barré, J., Benedictow, A., Blechschmidt, A.-M., … Suttie, M. (2019). The CAMS reanalysis of atmospheric composition. [Dataset] *Atmospheric Chemistry and Physics*, *19*(6), 3515–3556. https://doi.org/10.5194/acp-19-3515-2019

Inness, A., Ades, M., Agustí-Panareda, A., Barré, J., Benedictow, A., Blechschmidt, A.-M., … Suttie, M. (2019). The CAMS reanalysis of atmospheric composition. *Atmospheric Chemistry and Physics*, *19*(6), 3515–3556. https://doi.org/10.5194/acp-19-3515-2019

IPCC (2021). Summary for Policymakers. In: Climate Change 2021: The physical science basis. Contribution of working group I to the sixth assessment report of the intergovernmental panel on climate change [MassonDelmotte, V., P. Zhai, A. Pirani, S.L. Connors, C. Péan, S. Berger, N. Caud, Y. Chen, L. Goldfarb, M.I. Gomis, M. Huang, K. Leitzell, E. Lonnoy, J.B.R. Matthews, T.K. Maycock, T. Waterfield, O. Yelekçi, R. Yu, and B. Zhou (eds.)]. Cambridge University Press. In Press.

748 Japan Meteorological Agency (2019): Improvement and prospect of Global Spectral Model.
749 *Additonal Volume to Report of Numerical Prediction Division*, 65, 175 pp (in Japanese).
750 Jeong, G.-R. (2020). Weather effects of aerosols in the global forecast model. *Atmosphere*, *11*(8),
751 850. https://doi.org/10.3390/atmos11080850
752 Kajino, M., Deushi, M., Sekiyama, T. T., Oshima, N., Yumimoto, K., Tanaka, T. Y., Ching, J.,
753 Hashimoto, A., Yamamoto, T., Ikegami, M., Kamada, A., Miyashita, M., Inomata, Y.,
754 Shima, S. I., Takami, A., Shimizu, A., & Hatakeyama, S. (2019a). NHM-Chem, the Japan
755 meteorological agency's regional meteorology – chemistry model: Model evaluations
756 toward the consistent predictions of the chemical, physical, and optical properties of
757 aerosols. *Journal of the Meteorological Society of Japan*, *97*(2), 337–374.
758 https://doi.org/10.2151/JMSJ.2019-020
759 Kajino, M., Sekiyama, T. T., Igarashi, Y., Katata, G., Sawada, M., Adachi, K., Zaizen, Y.,
760 Tsuruta, H., & Nakajima, T. (2019b). Deposition and Dispersion of Radio-Cesium Released
761 Due to the Fukushima Nuclear Accident: Sensitivity to Meteorological Models and Physical
762 Modules. *Journal of Geophysical Research: Atmospheres*, *124*(3), 1823–1845.
763 https://doi.org/10.1029/2018JD028998
764 Kajino, M., Deushi, M., Sekiyama, T. T., Oshima, N., Yumimoto, K., Tanaka, T. Y., Ching, J.,
765 Hashimoto, A., Yamamoto, T., Ikegami, M., Kamada, A., Miyashita, M., Inomata, Y.,
766 Shima, S., Khatri, P., Shimizu, A., Irie, H., Adachi, K., Zaizen, Y., Igarashi, Y., Ueda, H.,
767 Maki, T., & Mikami, M. (2021a). Comparison of three aerosol representations of NHM-
768 Chem (v1.0) for the simulations of air quality and climate-relevant variables. *Geoscientific*
769 *Model Development*, 14(4), 2235–2264. https://doi.org/10.5194/gmd-14-2235-2021

Kajino, M., Tanji, N., & Kuramochi, M. (2021b). Better prediction of surface ozone by a superensemble method using emission sensitivity runs in Japan. *Atmospheric Environment: X*, *12*, 100120. https://doi.org/10.1016/j.aeaoa.2021.100120

Kaufman, Z. S., & Feldl, N. (2022). Causes of the Arctic's Lower-Tropospheric Warming Structure. *Journal of Climate*, *35*(6), 1983–2002. https://doi.org/10.1175/JCLI-D-21-0298.1

Kobayashi, S., Ota, Y., Harada, Y., Ebita, A., Moriya, M., Onoda, H., Onogi, K., Kamahori, H., Kobayashi, C., Endo, H., Miyaoka, K., & Takahashi, K. (2015). The JRA-55 reanalysis: general specifications and basic characteristics. [Dataset] *Journal of the Meteorological Society of Japan. Ser. II*, *93*(1), 5–48. https://doi.org/10.2151/jmsj.2015-001

Levy, R. C., Remer, L. A., Kleidman, R. G., Mattoo, S., Ichoku, C., Kahn, R., & Eck, T. F. (2010). Atmospheric Chemistry and Physics Global evaluation of the Collection 5 MODIS dark-target aerosol products over land. [Dataset] *Atmos. Chem. Phys*, *10*, 10399–10420. https://doi.org/10.5194/acp-10-10399-2010

Lohmann, U., & Feichter, J. (2005). Global indirect aerosol effects: a review. *Atmospheric Chemistry and Physics*, *5*(3), 715–737. https://doi.org/10.5194/acp-5-715-2005

Maki, T., Tanaka, T. Y., Sekiyama, T. T., & Mikami, M. (2011). The impact of ground-based observations on the inverse technique of aeolian dust aerosol. *Scientific Online Letters on the Atmosphere*, *7*(A), 21–24. https://doi.org/10.2151/sola.7A-006

Morcrette, J.-J., Boucher, O., Jones, L., Salmond, D., Bechtold, P., Beljaars, A., Benedetti, A., Bonet, A., Kaiser, J. W., Razinger, M., Schulz, M., Serrar, S., Simmons, A. J., Sofiev, M., Suttie, M., Tompkins, A. M., & Untch, A. (2009). Aerosol analysis and forecast in the European Centre for Medium-Range Weather Forecasts Integrated Forecast System:

Forward modeling. *Journal of Geophysical Research*, *114*(D6), D06206. https://doi.org/10.1029/2008JD011235

Mori, T., Kondo, Y., Ohata, S., Zhao, Y., Sinha, P. R., Oshima, N., Matsui, H., Moteki, N., & Koike, M. (2020). Seasonal Variation of Wet Deposition of Black Carbon in Arctic Alaska. *Journal of Geophysical Research: Atmospheres*, *125*(16). https://doi.org/10.1029/2019JD032240

Mori, T., Kondo, Y., Ohata, S., Goto-Azuma, K., Fukuda, K., Ogawa-Tsukagawa, Y., Moteki, N, Yoshida, A., Koike, M., Sinha, P. R., Oshima, N., Matsui, H., Tobo, Y., Yabuki, M. & Aas, W. (2021). Seasonal Variation of Wet Deposition of Black Carbon at Ny-Ålesund, Svalbard. *Journal of Geophysical Research: Atmospheres*, *126*(12). https://doi.org/10.1029/2020JD034110

Mulcahy, J. P., Walters, D. N., Bellouin, N., & Milton, S. F. (2014). Impacts of increasing the aerosol complexity in the Met Office global numerical weather prediction model. *Atmospheric Chemistry and Physics*, *14*(9), 4749–4778. https://doi.org/10.5194/acp-14-4749-2014

Niwano, M., Kajino, M., Kajikawa, T., Aoki, T., Kodama, Y., Tanikawa, T., & Matoba, S. (2021). Quantifying Relative Contributions of Light-Absorbing Particles From Domestic and Foreign Sources on Snow Melt at Sapporo, Japan During the 2011–2012 Winter. *Geophysical Research Letters*, *48*(16). https://doi.org/10.1029/2021GL093940

Perovich, D. K., Roesler, C. S., & Pegau, W. S. (1998). Variability in Arctic sea ice optical properties. *Journal of Geophysical Research: Oceans*, *103*(C1), 1193–1208. https://doi.org/10.1029/97JC01614

Porter, G. C. E., Adams, M. P., Brooks, I. M., Ickes, L., Karlsson, L., Leck, C., Salter, M. E., Schmale, J., Siegel, K., Sikora, S.N.F., Tarn, M. D., Vüllers, J., Wernli, H., Zieger, P., Zinke, J., Murray, B. J. (2022). Highly Active Ice-Nucleating Particles at the Summer North Pole. *Journal of Geophysical Research: Atmospheres*, *127*(6). https://doi.org/10.1029/2021JD036059

Randles, C. A., da Silva, A. M., Buchard, V., Colarco, P. R., Darmenov, A., Govindaraju, R., Smirnov, A., Holben, B., Ferrare, R., Hair, J., Shinozuka, Y., & Flynn, C. J. (2017). The MERRA-2 aerosol reanalysis, 1980 onward. Part I: System description and data assimilation evaluation. [Dataset] *Journal of Climate*, *30*(17), 6823–6850. https://doi.org/10.1175/JCLI-D-16-0609.1

Remer, L. A., Kaufman, Y. J., Tanré, D., Mattoo, S., Chu, D. A., Martins, J. V., … Holben, B. N. (2005). The MODIS aerosol algorithm, products, and validation. [Dataset] *Journal of the Atmospheric Sciences*, *62*(4), 947–973. https://doi.org/10.1175/JAS3385.1

Rémy, S., Benedetti, A., Bozzo, A., Haiden, T., Jones, L., Razinger, M., Flemming, J., Engelen, R. J., Peuch, V. H., & Thepaut, J. N. (2015). Feedbacks of dust and boundary layer meteorology during a dust storm in the eastern Mediterranean. *Atmospheric Chemistry and Physics*, *15*(22), 12909–12933. https://doi.org/10.5194/acp-15-12909-2015

Rémy, S., Kipling, Z., Flemming, J., Boucher, O., Nabat, P., Michou, M., Bozzo, A., Ades, M., Huijnen, V., Benedetti, A., Engelen, R., Peuch, V.-H., & Morcrette, J.-J. (2019). Description and evaluation of the tropospheric aerosol scheme in the European Centre for Medium-Range Weather Forecasts (ECMWF) Integrated Forecasting System (IFS-AER, cycle 45R1). Geoscientific Model Development, 12(11), 4627–4659. https://doi.org/10.5194/gmd-12-4627-2019

Rodwell, M. J., & Jung, T. (2008). Understanding the local and global impacts of model physics changes: an aerosol example. *Quarterly Journal of the Royal Meteorological Society*, *134*(635), 1479–1497. https://doi.org/10.1002/qj.298

Sato, K., & Inoue, J. (2021). Seasonal Change in Satellite-Retrieved Lower-Tropospheric Ice-Cloud Fraction Over the Southern Ocean. *Geophysical Research Letters*, *48*(23). https://doi.org/10.1029/2021GL095295

Schmale, J., Sharma, S., Decesari, S., Pernov, J., Massling, A., Hansson, H. C., Von Salzen, K., Skov, H., Andrews, E., Quinn, P. K., Upchurch, L. M., Eleftheriadis, K., Traversi, R., Gilardoni, S., Mazzola, M., Laing, J. Hopke, P. (2022). Pan-Arctic seasonal cycles and long-term trends of aerosol properties from 10 observatories. *Atmospheric Chemistry and Physics*, *22*(5), 3067–3096. https://doi.org/10.5194/acp-22-3067-2022

Sekiyama, T. T., Tanaka, T. Y., Shimizu, A., & Miyoshi, T. (2010). Data assimilation of CALIPSO aerosol observations. *Atmospheric Chemistry and Physics*, *10*(1), 39–49. https://doi.org/10.5194/acp-10-39-2010

Serreze, M. C., & Barrett, A. P. (2008). The summer cyclone maximum over the central Arctic Ocean. *Journal of Climate*, *21*, 1048–1065. https://doi.org/10.1175/2007JCLI1810.1

Simmonds, I., & Rudeva, I. (2012). The great Arctic cyclone of August 2012. *Geophysical Research Letters*, *39*(23), 1–6. https://doi.org/10.1029/2012GL054259

Stohl, A. (2006). Characteristics of atmospheric transport into the Arctic troposphere. *Journal of Geophysical Research Atmospheres*, *111*(11). https://doi.org/10.1029/2005JD006888

Stohl, A., Andrews, E., Burkhart, J. F., Forster, C., Herber, A., Hoch, S. W., … Yttri, K. E. (2006). Pan-Arctic enhancements of light absorbing aerosol concentrations due to North

American boreal forest fires during summer 2004. *Journal of Geophysical Research Atmospheres*, *111*(22). https://doi.org/10.1029/2006JD007216

Stohl, A., Klimont, Z., Eckhardt, S., Kupiainen, K., Shevchenko, V. P., Kopeikin, V. M., & Novigatsky, A. N. (2013). Black carbon in the Arctic: the underestimated role of gas flaring and residential combustion emissions. *Atmospheric Chemistry and Physics*, *13*(17), 8833–8855. https://doi.org/10.5194/acp-13-8833-2013

Sugimoto, N., Hara, Y., Yumimoto, K., Uno, I., Nishikawa, M., & Dulam, J. (2010). Dust emission estimated with an assimilated dust transport model using lidar network data and vegetation growth in the Gobi Desert in Mongolia. *SOLA*, *6*(1), 125–128. https://doi.org/10.2151/sola.2010-032

Tanaka, T. Y., Orito, K., Sekiyama, T. T., Shibata, K., Chiba, M., & Tanaka, H. (2003). MASINGAR, a global tropospheric aerosol chemical transport model coupled with MRI/JMA98 GCM: Model description. *Papers in Meteorology and Geophysics*, *53*(4), 119–138. https://doi.org/10.2467/mripapers.53.119

Tanaka, T. Y., & Chiba, M. (2005). Global simulation of dust aerosol with a chemical transport model, MASINGAR. *Journal of the Meteorological Society of Japan*, *83*(3), 255–278. https://doi.org/10.2151/jmsj.83a.255

Tanaka, H. L. L., Yamagami, A., & Takahashi, S. (2012). The structure and behavior of the arctic cyclone in summer analyzed by the JRA-25/JCDAS data. Polar Science, 6(1), 55–69. https://doi.org/10.1016/j.polar.2012.03.001

Tian, J., Chen, X., Cao, Y., & Chen, F. (2022). Satellite Observational Evidence of Contrasting Changes in Northern Eurasian Wildfires from 2003 to 2020. *Remote Sensing*, *14*(17), 4180. https://doi.org/10.3390/rs14174180

Tilinina, N., Gulev, S. K., & Bromwich, D. H. (2014). New view of Arctic cyclone activity from the Arctic system reanalysis. Geophysical Research Letters, 41(5), 1766–1772. https://doi.org/10.1002/2013GL058924

Vessey, A. F., Hodges, K. I., Shaffrey, L. C., & Day, J. J. (2020). An inter-comparison of Arctic synoptic scale storms between four global reanalysis datasets. Climate Dynamics, 54(5–6), 2777–2795. https://doi.org/10.1007/s00382-020-05142-4

Warren, S. G., & Wiscombe, W. J. (1980). A model for the spectral albedo of snow. II: Snow containing atmospheric aerosols. Journal of the Atmospheric Sciences, 37, 2734–2745. https://doi.org/10.1175/1520-0469(1980)037<2734:AMFTSA>2.0.CO;2

Xian, P., Zhang, J., O'Neill, N. T., Toth, T. D., Sorenson, B., Colarco, P. R., … Ranjbar, K. (2022). Arctic spring and summertime aerosol optical depth baseline from long-term observations and model reanalyses – Part 1: Climatology and trend. *Atmospheric Chemistry and Physics*, *22*(15), 9915–9947. https://doi.org/10.5194/acp-22-9915-2022

Yamagami, A., Matsueda, M., & Tanaka, H. L. (2017). Extreme Arctic cyclone in August 2016. *Atmospheric Science Letters*, *18*(7), 307–314. https://doi.org/10.1002/asl.757

Yamagami, A., Matsueda, M., & Tanaka, H. L. (2018a). Predictability of the 2012 Great Arctic Cyclone on medium-range timescales. Polar Science, 15, 13–23. https://doi.org/10.1016/j.polar.2018.01.002

Yamagami, A., Matsueda, M., & Tanaka, H. L. (2018b). Medium-range forecast skill for extraordinary Arctic cyclones in summer of 2008–2016. *Geophysical Research Letters*, *45*(9), 4429–4437. https://doi.org/10.1029/2018GL077278

Yamagami, A., & Matsueda, M. (2021). Statistical characteristics of Arctic forecast busts and their relationship to Arctic weather patterns in summer. *Atmospheric Science Letters*, *March*. https://doi.org/10.1002/asl.1038

Yamagami, A., Kajino, M., & Maki, T. (2022). Statistical Evaluation of the Temperature Forecast Error in the Lower-Level Troposphere on Short-Range Timescales Induced by Aerosol Variability. *Journal of Geophysical Research: Atmospheres*, 1–19. https://doi.org/10.1029/2022jd036595

Yamashita, Y., Takigawa, M., Goto, D., Yashiro, H., Satoh, M., Kanaya, Y., Taketani, F., & Miyakawa, T. (2021). Effect of model resolution on black carbon transport from Siberia to the arctic associated with the well-developed low-pressure systems in september. *Journal of the Meteorological Society of Japan*, *99*(2), 287–308. https://doi.org/10.2151/jmsj.2021-014

Yoshimori, M., Abe-ouchi, A., Watanabe, M., Oka, A., & Ogura, T. (2014). Robust Seasonality of Arctic Warming Processes in Two Different Versions of the MIROC GCM. *Journal of Climate*, *27*(16), 6358–6375. https://doi.org/10.1175/JCLI-D-14-00086.1

Yukimoto, S., H. Yoshimura, M. Hosaka, T. Sakami, H. Tsujino, M. Hirabara, T. Y. Tanaka, M. Deushi, A. Obata, H. Nakano, Y. Adachi, E. Shindo, S. Yabu, T. Ose, and A. Kitoh, (2011). Meteorological Research Institute Earth System Model Version 1 (MRI-ESM1)—Model Description—. *Tech. Rep. of MRI*, 64, 83 pp.

Yukimoto, S., Adachi, Y., Hosaka, M., Sakami, T., Yoshimura, H., Hirabara, M.,Tanaka, T. Y., Shindo, E., Tsujino, H., Deushi, M., Mizuta, R., Yabu, S., Obata, A., Nakano, H., Koshiro, T., Ose, T., & Kitoh, A. (2012). A New Global Climate Model of the Meteorological Research Institute: MRI-CGCM3 —Model Description and Basic Performance—. *Journal*

of the Meteorological Society of Japan. Ser. II, *90A*(A), 23–64. https://doi.org/10.2151/jmsj.2012-A02

Yumimoto, K., Uno, I., Sugimoto, N., Shimizu, A., Liu, Z., & Winker, D. M. (2008). Adjoint inversion modeling of Asian dust emission using lidar observations. *Atmospheric Chemistry and Physics*, *8*(11), 2869–2884. https://doi.org/10.5194/acp-8-2869-2008

Yumimoto, K., Nagao, T. M., Kikuchi, M., Sekiyama, T. T., Murakami, H., Tanaka, T. Y., Ogi, A., Irie, H., Khatri, P., Okumura, H., Arai, K., Morino, I., Uchino, O., & Maki, T. (2016). Aerosol data assimilation using data from Himawari-8, a next-generation geostationary meteorological satellite. *Geophysical Research Letters*, *43*(11), 5886–5894. https://doi.org/10.1002/2016GL069298

Yumimoto, K., Tanaka, T. Y., Oshima, N., & Maki, T. (2017). JRAero: the Japanese Reanalysis for Aerosol v1.0. [Dataset] *Geoscientific Model Development*, *10*(9), 3225–3253. https://doi.org/10.5194/gmd-10-3225-2017

Zhang, J., Reid, J. S., Christensen, M., & Benedetti, A. (2016). An evaluation of the impact of aerosol particles on weather forecasts from a biomass burning aerosol event over the Midwestern United States: observational-based analysis of surface temperature. *Atmospheric Chemistry and Physics*, *16*(10), 6475–6494. https://doi.org/10.5194/acp-16-6475-2016

Zhang, X., Walsh, J. E., Zhang, J., Bhatt, U. S., & Ikeda, M. (2004). Climatology and interannual variability of Arctic cyclone activity: 1948-2002. *Journal of Climate*, *17*, 2300–2317. https://doi.org/10.1175/1520-0442(2004)017<2300:CAIVOA>2.0.CO;2

Journal of Geophysical Research: Atmosphere

Supporting Information for

Spatiotemporal variations in summertime Arctic aerosol optical depth caused by synoptic-scale atmospheric circulation in three reanalyses

A. Yamagami[1], M. Kajino[1,2], T. Maki[1], and T. Toyoda[1]

1 Meteorological Research Institute (MRI), Japan Meteorological Agency (JMA), Tsukuba, Ibaraki, 305-0052, Japan

2 Faculty of Life and Environmental Sciences, University of Tsukuba, Tsukuba, Ibaraki, 305-8572, Japan

Contents of this file

Introduction

This supporting information includes the following figures:

- Distribution in the contribution of each aerosol species to total AOD in JRAero, CAMSRA, and MERRA-2 over north of 60ºN (Fig. S1);
- An example of the relationship between SLP and AOD for the case of AC in August 2016. (Fig. S2);
- Difference in SLP and emission of organic carbon between high and low loading days. (Fig. S3);
- Total AOD and sulfate, black carbon, organic carbon, dust, and sea salt aerosol contributions regressed on to PC-1 in JRAero (Fig. S4);
- Dry and wet deposition fluxes of OC and SS in MERRA2 regressed onto PC-1 (Fig. S5);
- Similar to those in Fig. S4, but for PC-2 (Fig. S6).

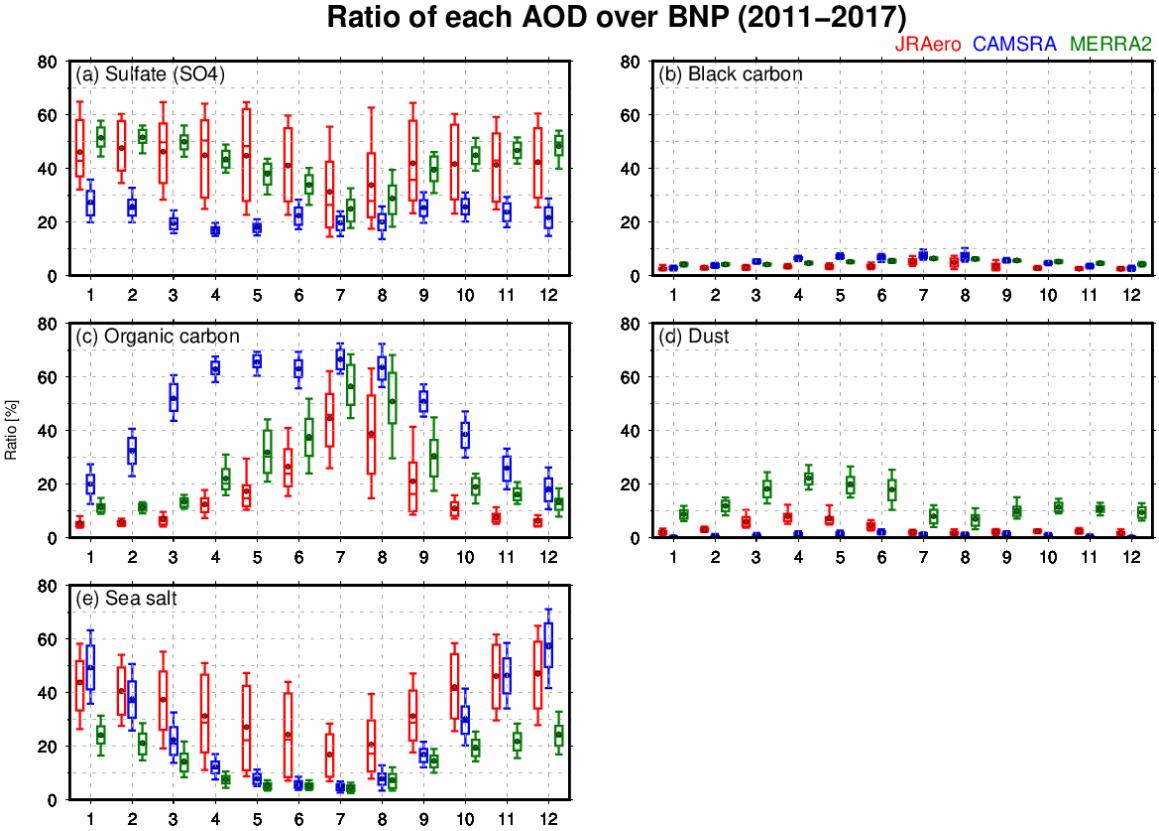

Figure S1. Similar to Fig. 2, bur for the ratio to the total AOD.

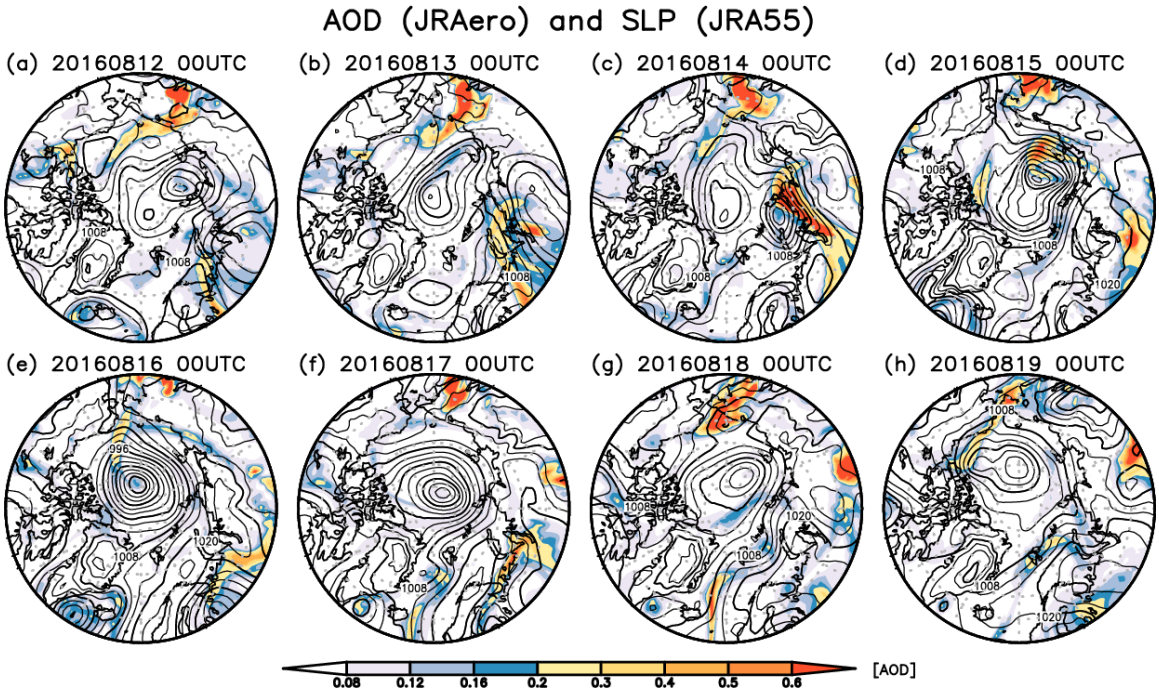

Figure S2. Similar to Fig. 5, bur for the AC in August 2016 in the time interval of 1 day from 00UTC on (a) 12 August to (h) 19 August 2017.

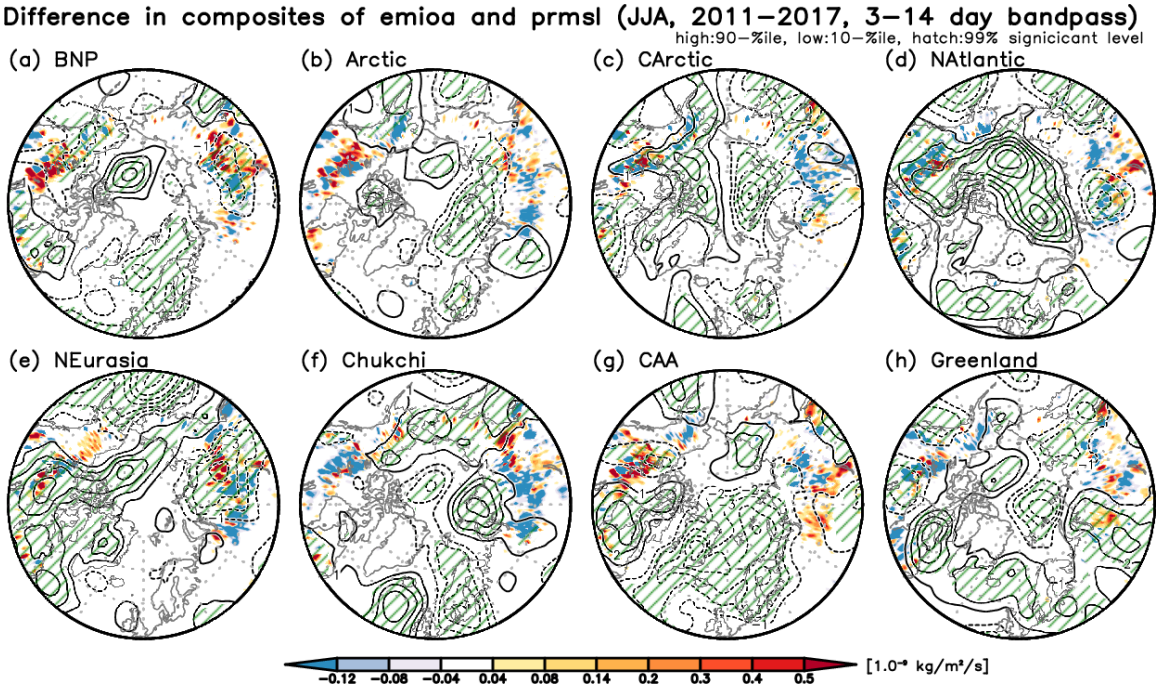

Figure S3. Similar to Fig. 6, but for difference in SLP (contour) and emission of OC (shading).

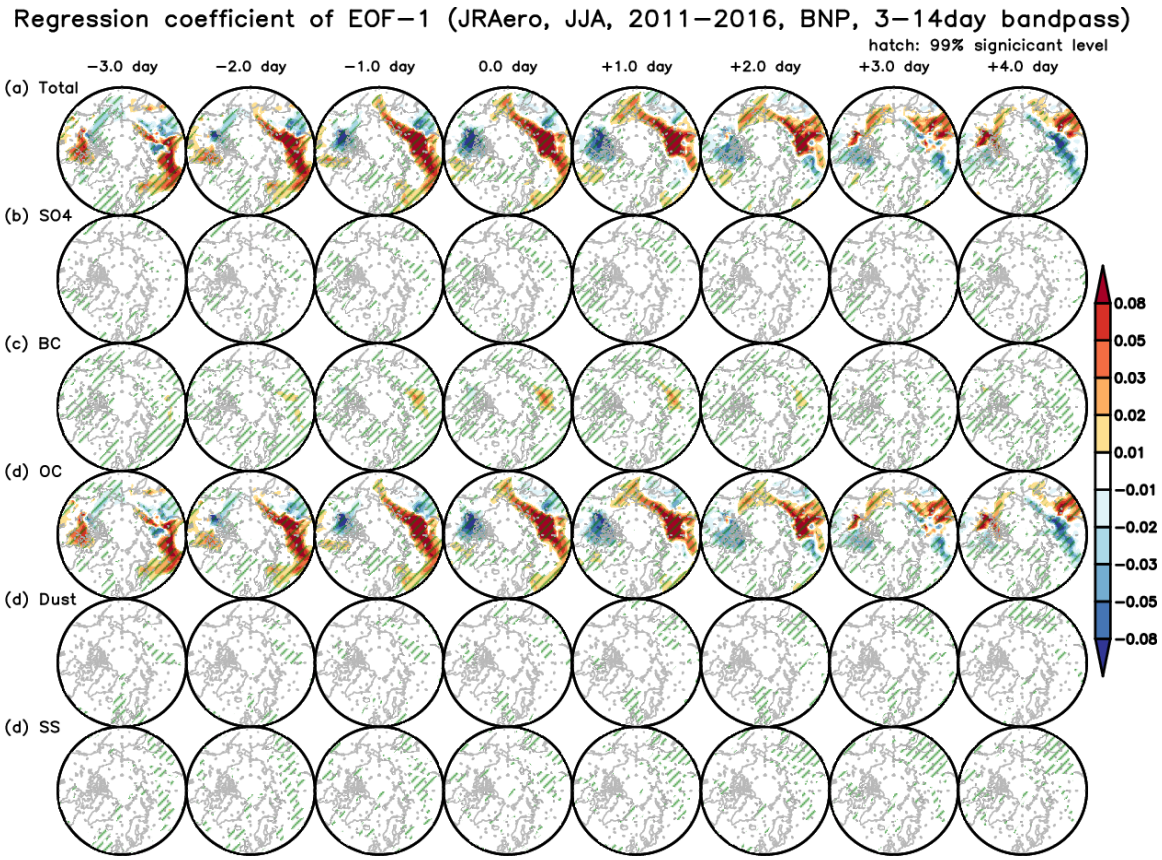

Figure S4. Similar to Fig. 9a, but for (a) total, (b) Sulfate (SO4), (c) black carbon (BC), (d) organic carbon (OC), (e) Dust, and (f) sea salt (SS) aerosol contributions.

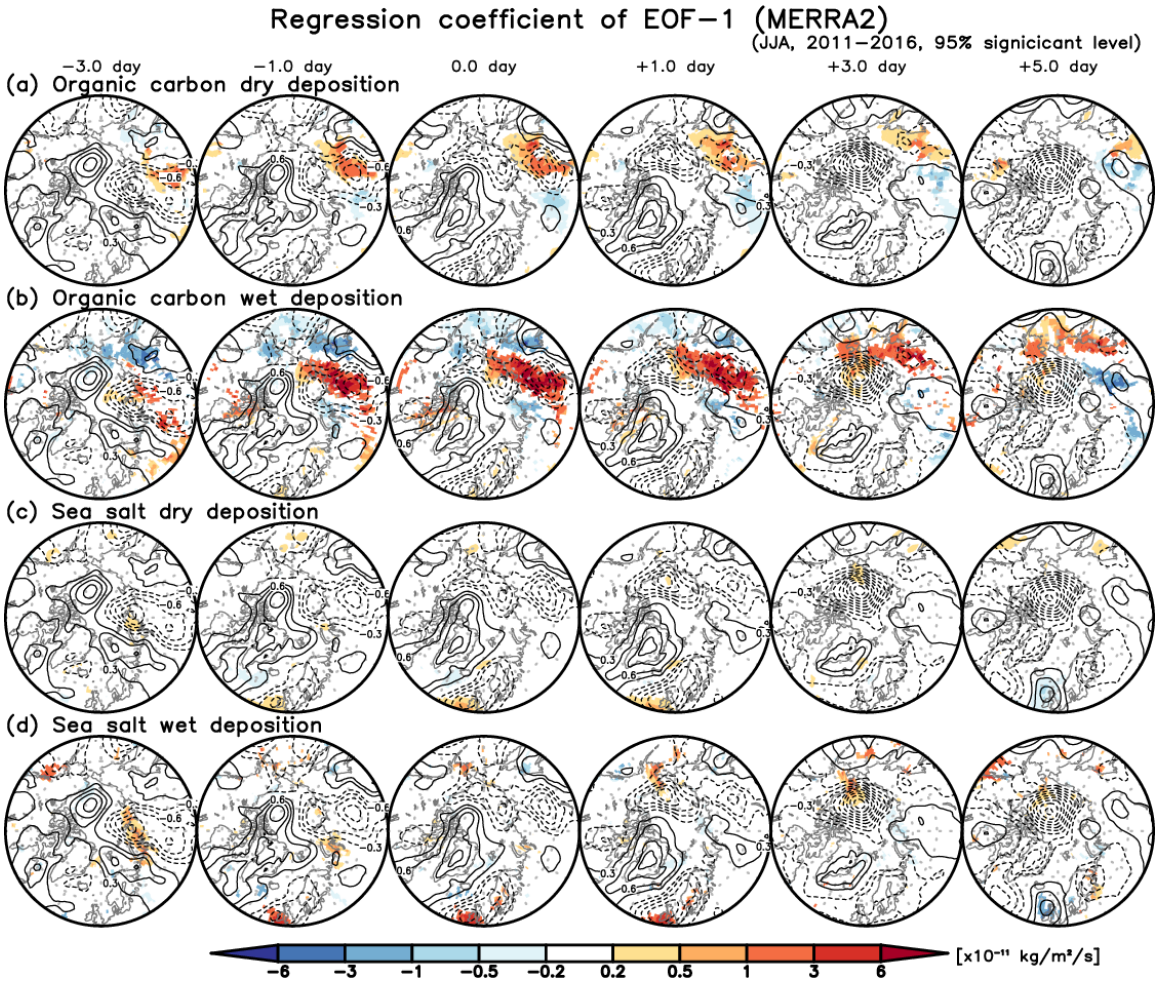

Figure S5. Similar to Fig. 10, bur for MERRA2.

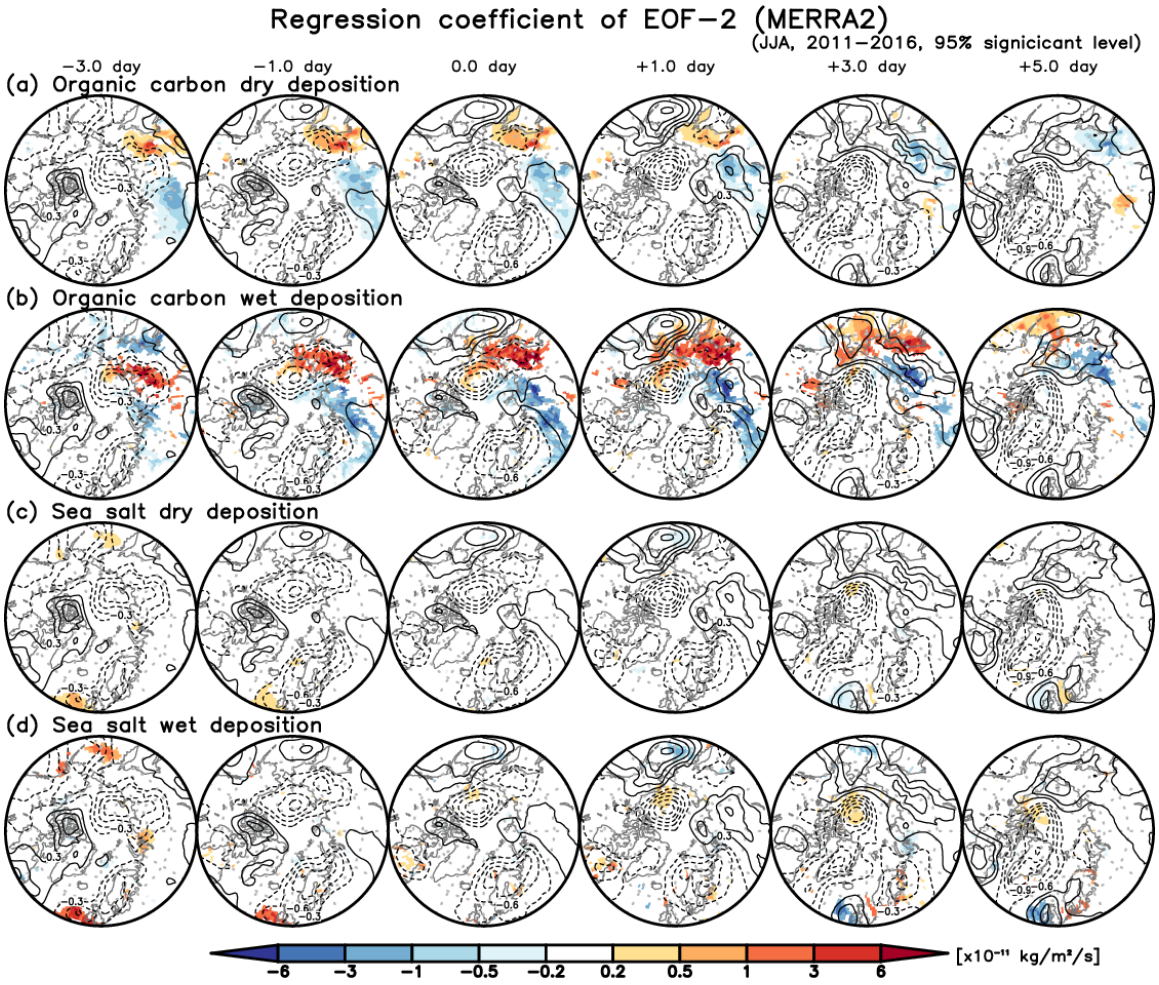

Figure S6. Similar to Fig S4, but for PC-2.